Advances in Nano Research, *Vol. 12, No. 1 (2022) 81-99*
https://doi.org/10.12989/anr.2022.12.1.081

A machine learning-based model for the estimation of the critical thermo-electrical responses of the sandwich structure with magneto-electro-elastic face sheet

Xiao Zhou[1], Pinyi Wang*[2], Mujahed Al-Dhaifallah[3,4], Muhyaddin Rawa[5,6,7] and Mohamed Amine Khadimallah[8,9]

[1]*College of science, Hubei University of Automotive Technology, Shiyan, 442002, Hubei, China*
[2]*Department of Electrical and Computer Engineering, University of Washington Seattle, WA 98195, USA*
[3]*Control and Instrumentation Engineering Department, King Fahd University of Petroleum & Minerals, 31261 Dhahran, KSA*
[4]*Interdisciplinary Research Center (IRC) for Renewable Energy and Power Systems, King Fahd University of Petroleum & Minerals, 31261 Dhahran, KSA*
[5]*Center of Research Excellence in Renewable Energy and Power Systems, King Abdulaziz University, Jeddah 21589, Saudi Arabia*
[6]*K. A. CARE Energy Research and Innovation Center, King Abdulaziz University, Jeddah 21589, Saudi Arabia*
[7]*Department of Electrical and Computer Engineering, Faculty of Engineering, King Abdulaziz University, Jeddah 21589, Saudi Arabia*
[8]*Prince Sattam Bin Abdulaziz University, College of Engineering, Civil Engineering Department, Al-Kharj, 16273, Saudi Arabia*
[9]*Laboratory of Systems and Applied Mechanics, Polytechnic School of Tunisia, University of Carthage, Tunis, Tunisia*

(*Received April 13, 2021, Revised October 19, 2021, Accepted December 14, 2021*)

Abstract. The aim of current work is to evaluate thermo-electrical characteristics of graphene nanoplatelets Reinforced Composite (GNPRC) coupled with magneto-electro-elastic (MEE) face sheet. In this regard, a cylindrical smart nanocomposite made of GNPRC with an external MEE layer is considered. The bonding between the layers are assumed to be perfect. Because of the layer nature of the structure, the material characteristics of the whole structure is regarded as graded. Both mechanical and thermal boundary conditions are applied to this structure. The main objective of this work is to determine critical temperature and critical voltage as a function of thermal condition, support type, GNP weight fraction, and MEE thickness. The governing equation of the multilayer nanocomposites cylindrical shell is derived. The generalized differential quadrature method (GDQM) is employed to numerically solve the differential equations. This method is integrated with Deep Learning Network (DNN) with ADADELTA optimizer to determine the critical conditions of the current sandwich structure. This the first time that effects of several conditions including surrounding temperature, MEE layer thickness, and pattern of the layers of the GNPRC is investigated on two main parameters critical temperature and critical voltage of the nanostructure. Furthermore, Maxwell equation is derived for modeling of the MEE. The outcome reveals that MEE layer, temperature change, GNP weight function, and GNP distribution patterns GNP weight function have significant influence on the critical temperature and voltage of cylindrical shell made from GNP nanocomposites core with MEE face sheet on outer of the shell.

Keywords: critical temperature; critical voltage; deep learning network; graphene nanoplatelets; neural network

1. Introduction

GNP reinforcement has drawn substantial attention in recent years. Composites with GNP as their reinforcement components has considerable applications; some of them are presented in Ref. (Habibi *et al*. 2018a, 2019a, b, c, Shi *et al*. 2018, Pourjabari *et al*. 2019, Safarpour *et al*. 2019a, Moayedi *et al*. 2020a, Shokrgozar *et al*. 2020a). In their experiments, Sun and Zhao (Habibi *et al*. 2016, 2018b, Sun and Zhao 2018, Ebrahimi *et al*. 2019, Esmailpoor Hajilak *et al*. 2019, Ghabussi *et al*. 2019, Safarpour *et al*. 2020a, Shariati *et al*. 2020a) reinforced functionally graded cemented carbide with multi-layer graphenes (MLGs) and compared the differences in fracture characteristics with the same material without reinforcement. It was shown that the MLG with opposite gradients to cobalt gradients generates compressive surface residual stresses. Checchetto *et al*. (2014) investigated the interesting application of GNPs in the permeability of polyethylene membrane. The gas separation and gas barrier properties of membranes produced using distributed GNPs in a matrix of low-density polyethylene. It is noteworthy, the GPL refinement affects the mechanical behavior (Tounsi *et al*. 2013, Salari 2016, Ebrahimi and Jafari 2017, Ehyaei and Daman 2017, Kumar 2018, Wu *et al*. 2018, Ebrahimi *et al*. 2019a, b, Ebrahimi and Salari 2019, Emdadi *et al*. 2019, Ghannadpour and Moradi 2019, Shahsavari *et al*. 2019, Dehshahri *et al*. 2020, Zhu *et al*. 2020). Refs (Rafiee *et al*. 2009, Habibi *et al*. 2019d, Safarpour *et al*. 2019b, Al-Furjan *et al*. 2020a, Alipour *et al*. 2020, Ebrahimi *et al*. 2020, Ghabussi *et al*. 2020) evaluated the behavior of three types of epoxy nanocomposites reinforced with GNP, single-walled carbon nanotubes, multi-walled carbon nanotube. It was indicated that the material characteristics of GNP nanocomposites, including elastic, fracture, and fatigue behaviors, are improved compared with the other ones. Thus, they

*Corresponding author, Ms.,
E-mail: wpy1029@uw.edu

ISSN: 2287-237X (Print), 2287-2388 (Online)

concluded that in place of SWNTs and MWNTs, GNP could be added to the epoxy in nanocomposites. Notably, the application of nanomaterials stiffened by GNP is more preferable in design. In consequence, more light is shed on the importance of dynamic modeling of the GNP nanocomposite. The bucking and post-buckling behavior of beams composed of functionally graded multilayer GNP nanocomposites were presented by Yang *et al*. (2017). The results reveal that adding GNPs to the matrix enhanced the buckling and post-buckling characteristics of the beams produced by these nanocomposites. In another study, the bending of new class beams composed of multi-layer polymer composite beams reinforced by GNPs was investigated (Feng *et al*. 2017). They showed that, in nonlinear deformations, the sensitivity of beams with asymmetric dispersion and greater volume fraction of GNPs are less. In engineering macro structures, some researches showed that adding nano-materials leads to enhancement of the mechanical properties at the macro-scale structures.

Dynamical behavior of piezoelectric cylindrical shells was also attracted attention of researchers (Habibi *et al*. 2017, 2019a, Safarpour *et al*. 2018, 2019a, 2020b, Ghazanfari *et al*. 2020, Jermsittiparsert *et al*. 2020). Dehkordi and Beni (2017), with the aid of Love's cylindrical model and couple stress theory, investigated the free vibrations of the isotropic conic nanotubes. These tubes are made of a single wall nanotube with piezoelectric layers. Kheibari and Beni (2017) also worked on the free vibrations of piezoelectric nanotube using the same theory. In this paper, the governing equations of deformation, size effects, electro-mechanical and geometric parameters influencing the nanotubes' natural frequency are discussed. Arefi (2018) utilized the nonlocal elasticity theories to analyze electro-elastic bending of a doubly curved nanoshell. Transverse loads and voltage are applied on the nanoshell surrounded by the Winkler-Pasternak foundation. In the mentioned work, the influences of the applied electric potential nonlocal parameter, Winkler and Pasternak's parameters, on the behavior of the piezoelectric nanoshells were examined from both mechanical and electrical points of view. In another paper on piezoelectric nanoshell, Razavi *et al*. (Razavi *et al*. 2017) modeled FG and piezoelectric composed nanoshells. They described how the variation of geometrical and size effect parameters influence the vibrational behavior of the nanoshells. Ninh and Bich (2018) investigated the effect of electro-thermo-mechanical applied loads on the vibration of the nanocomposite cylinders. In this regard, the inner and outer surfaces of carbon nanotube reinforced an FG composite nanoshell covered with piezoelectric layers is considered. The applied covering piezoelectric layers worked as actuators. The Runge-Kutta method (Ebrahimi *et al*. 2019a, b, 2020, Mohammadgholiha *et al*. 2019, Mohammadi *et al*. 2019a, Habibi *et al*. 2020, Shariati *et al*. 2020b, Shokrgozar *et al*. 2020b) is employed to acquire semi-analytical results and natural frequencies, responses of the nanostructures, relation of frequency ratios–amplitudes are presented. Furthermore, effects of the volume fraction percent of the CNTs, thermal condition, number of piezoelectric layers, reinforcement pattern distribution, geometrical parameters, and properties of elastic foundation are investigated in a parametric study. In a similar study, Fang and Zhou (2017) investigated the effect of piezoelectric layer on nanoshell's free vibration. They employed the electro-elastic surface/ interface theories along with Donnell's nonlinear shallow-shell for exploring vibrations and size effects. In addition, the surface material characteristics and residual volume stress were engaged in investigating their effects on the vibrations of the nanocomposites. Eftekhari *et al*. (2018) investigated natural frequencies of temperature-dependent FG piezoelectric nanostructures with carbon nanotubes as reinforcement embedded in an orthotropic elastic medium. They presented influences of distribution pattern, magnetic and electrical loads on the dynamic behaviors of the nanostructures employing analytical and numerical solutions. Mohammadimehr *et al*. (2018) presented the vibrational behavior of a magneto-electro-elastic nanotube. They employed the first-order shear deformation theory, and the open and closed circuits boundary conditions were considered. The outcomes of the study indicated that the free vibrations characteristics of the nanotubes endured significant changes due to the value and pattern of distribution of CNTs. In another study, Zhu *et al*. (2017) investigated the free vibrations of the cylindrical nanoshells with piezoelectric layers considering nonlinear effects under electro-elastic forces. The perturbation method was utilized to solve nonlinear equations. Singh and Panda (2017) numerically solved the equations of a curved piezoelectric nanoshell panel. The results reveal that the vibrational characteristics of the nanoshell were influenced by the number of piezoelectric layers. Fan *et al*. (2017) studied the vibrational behavior of a CNTRC piezoelectric conical nanostructure. The focus in this study was on how the free vibration behavior of the nanostructure varies with variations in the volume fractions as well as distribution types of CNT and surrounding conditions including boundary and temperture. There is also one another interesting field in the rotating behavior of nanostructures. The dynamic stability of rotating cylindrical nanoshell in electro-magnetic fields was investigated by Shojaeefard *et al* (2018). They considered the influences of electrical field, angular velocities, magnetic field and elastic foundation on the free vibration of the nanoshell. In a study, two directional FG piezoelectric circular nanoplates was examined in the rotating state by Mahinzare *et al*. (2018). In this research, they incorporated velocity, external electric voltage, size and power-law index in the equations to analyze the vibrational characteristics of nanoplates. Mohammadi *et al*. (2019b) used the modified couple stress theory to formulate a size-dependent three-dimensional dynamic model. They utilize this model to study micro double-wall shell and the its natural frequencies affected by FG power index, length, shear correction factor, thickness and Winkler and Pasternak coefficients.

Consequently, critical voltage and critical temperature of the cylindrical sandwich shell with GNPRC core and MEE face sheet attracts significant appeal through physics-informed neural networks. To the best of the authors' knowledge, no study has been reported concerning the critical voltage and temperature of a GNPRC cylindrical

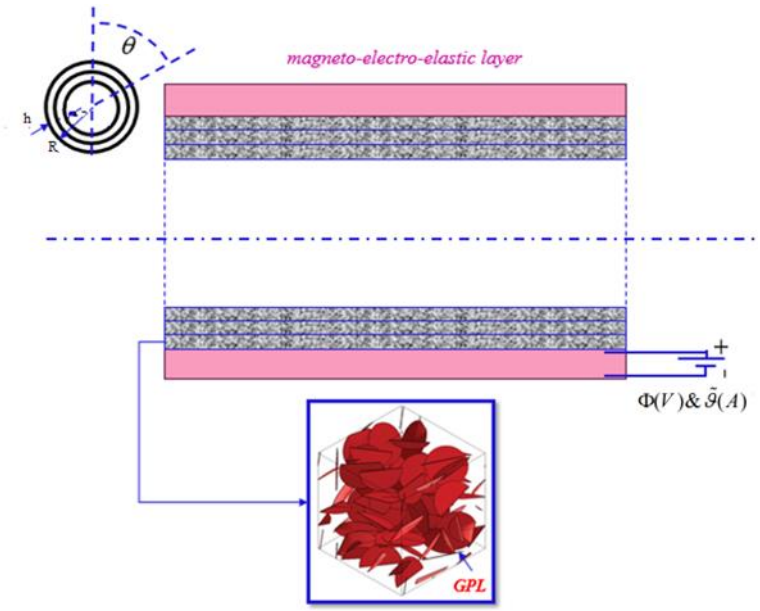

Fig. 1 Schematic representation of the sandwich shell coupled with MEE layer

Table 1 Convergence test of the sandwich structure for different number of grid point in different boundary conditions

B. Cs	Material	N = 5	N = 7	N = 9	N = 11	N = 13
S-S	Pure epoxy	1258.659	1256.622	1256.856	1256.856	1256.856
	Pattern 4	1785.632	1783.652	1783.652	1783.652	1783.652
C-S	Pure epoxy	1453.659	1452.365	1452.958	1452.958	1452.958
	Pattern 4	2150.639	2148.326	2149.635	2149.635	2149.635
C-C	Pure epoxy	1658.639	1654.236	1654.636	1654.636	1654.636
	Pattern 4	2356.652	2355.659	2357.863	2357.863	2357.863

shell coupled with MEE layer. The governing equation of the multilayer nanocomposites cylindrical shell is derived. The generalized differential quadrature method (GDQM) (Hashemi *et al*. 2019, Moayedi *et al*. 2019, 2020b, c, Oyarhossein *et al*. 2020, Shariati *et al*. 2020c) is employed to numerically solve the differential equations. This method is integrated with Deep Learning Network (DNN) with ADADELTA optimizer to determine the critical conditions of the sandwich structure. This is the first time that effects of several conditions, including surrounding temperature, MEE layer thickness, and pattern of the layers of the GNPRC are investigated on two main parameters critical temperature and critical voltage of the sandwich structure. Furthermore, Maxwell equation is derived for modeling the MEE layer. Finally, the results show that some geometrical and physical parameters have an important role in the critical voltage and temperature of the current sandwich structure.

2. Governing equations

In Fig. 1, a cylindrical shell coupled with MEE layer in a thermal circumstance is shown. Also, the core of the current structure is reinforced by GNPs (Azoti and Elmarakbi 2019). The parameters $h(h_C+h_M)$, L, and R are thickness, length, and the middle surface radius of the cylindrical shell, respectively. In addition, the electric potential (Φ) and magnetic potential ($\eth$) is applied to the structure. The core of the shell is made of composite material.

2.1 Core of the composite

As shown in Fig. 1, the composite core is GNPRC materials. The volume fraction of the components are as follows:

$$U - GNPRC: V_{GNP}(k) = V_{GNP}^{*} \quad (1)$$

$$X - GNPRC: V_{GNP}(k) = 2V_{GNP}^{*}\frac{1}{N_L}|2k - 1 - N_L| \quad (2)$$

$$O - GNPRC: V_{GNP}(k) = 2V_{GNP}^{*}\left[1 - \frac{1}{N_L}|2k - 1 - N_L|\right] \quad (3)$$

$$A - GNPRC: V_{GNP}(k) = \frac{2}{N_L}(2k - 1)V_{GNP}^{*} \quad (4)$$

in which the layer number, total number of layers, and the overall GNPs volume fraction are denoted by k, N_L and

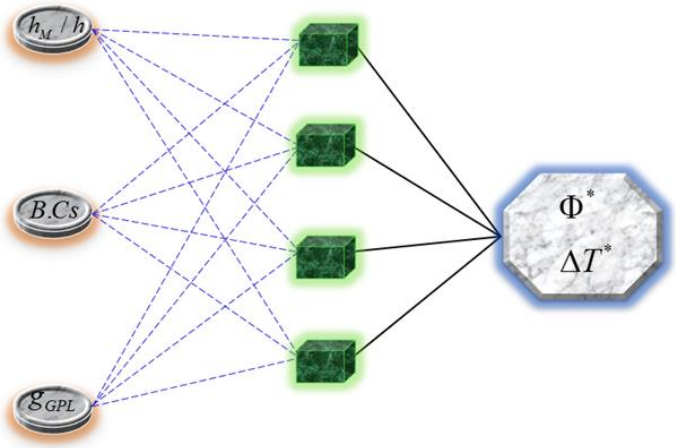

Fig. 1 Configuration of the system of the fully-connected DNN

V^*_{GPL}, respectively. The dependence of V^*_{GNP} on the weight fraction g_{GNP} is (Hashemi *et al*. 2019, Al-Furjan *et al*. 2020b, Cheshmeh *et al*. 2020, Lori *et al*. 2020, Najaafi *et al*. 2020, Shariati *et al*. 2020d):

$$V^*_{GNP} = \frac{g_{GNP}}{g_{GNP} + (\rho_{GNP}/\rho_m)(1 - g_{GNP})} \tag{5}$$

where ρ_m is the density of matrix and ρ_{GNP} is the GNP's density. According to Halpin-Tsai model, the equivalent modulus of elasticity E of the randomly dispersed GNP composite layers can be represented by the following relation (Song *et al*. 2017):

$$\begin{aligned} E &= \frac{3}{8}E_L + \frac{5}{8}E_T, \\ E_L &= \frac{1 + \xi_L n_L V_{GNP}}{1 - n_L V_{GNP}}E_m, E_T = \frac{1 + \xi_T n_T V_{GNP}}{1 - n_T V_{GNP}}E_m \end{aligned} \tag{6}$$

where E is the effective modulus of composites layer, and E_L and E_T are the longitudinal and transverse elastic moduli for a lamina with parallel reinforcement. The parameters n_L and n_T with geometry factors of GNPs (ξ_L and ξ_T) are defined by (Al-Furjan *et al*. 2020c, d, Bai *et al*. 2020, Zhang *et al*. 2021c, Zhong *et al*. 2020, Guo *et al*. 2021a, Liu *et al*. 2021):

$$\begin{aligned} &\xi_L = 2(l_{GNP}/h_{GNP}), \xi_t = 2(b_{GNP}/h_{GNP}), \\ &n_L = \frac{(E_{GNP}/E_m) - 1}{(E_{GNP}/E_m) + \xi_L}, n_T = \frac{(E_{GNP}/E_m) - 1}{(E_{GNP}/E_m) + \xi_T} \end{aligned} \tag{7}$$

In these definitions, the geometrical parameters of GNPs are average length l_{GPL}, thickness h_{GPL} and width b_{GPL}. The equivalent elastic module (E), equivalent density (ρ), and equivalent poisson's ratio (ν), and equivalent thermal expansion factor (α) of the composite can be obtained using the rule of mixtures:

$$\begin{aligned} E &= E_{GNP}V_{GNP} + E_M V_M, \\ \rho &= \rho_{GNP}V_{GNP} + \rho_M V_M, \\ \nu &= \nu_{GNP}V_{GNP} + \nu_M V_M, \\ \alpha &= \alpha_{GNP}V_{GNP} + \alpha_M V_M. \end{aligned} \tag{8}$$

where $V_M = 1 - V_{GNP}$.

2.2 Kinematic equations of the core

A two-dimensional formulation is extracted from three-dimensional elasticity equations using Taylor's expansion, and the subsequent equations are derived by considering the displacement components at any point in the laminate space as a linear function of thickness coordinate z. Also, small deformations and rotations are assumed throughout this study. Thus,

$$\begin{aligned} u_c(z,x,t,\theta) &= u_{0c}(x,t,\theta) + z{\psi^c}_x(x,t,\theta) \\ v_c(z,x,t,\theta) &= v_{0c}(x,t,\theta) + z{\psi^c}_\theta(x,t,\theta) \\ w_c(z,x,t,\theta) &= w_{0c}(x,t,\theta) \end{aligned} \tag{9}$$

where, displacement variables of middle surface are axial u_{0c}, circumferential v_{0c}, and radial w_{0c} displacements. Two functions ${\psi^c}_\theta$ and ${\psi^c}_x$ are the rotation functions about axial and circumferential directions, respectively, of the normal vector to the middle plane.

2.3 Elasticity equations of composite core

The linear elasticity equations of the cylindrical sandwich shell with composite core are as follows:

$$\begin{bmatrix} {\sigma^c}_{xx} \\ {\sigma^c}_{\theta\theta} \\ {\sigma^c}_{x\theta} \\ {\sigma^c}_{xz} \\ {\sigma^c}_{\theta z} \end{bmatrix} = \begin{bmatrix} \bar{Q}_{11} & \bar{Q}_{12} & 0 & 0 & 0 \\ \bar{Q}_{21} & \bar{Q}_{22} & 0 & 0 & 0 \\ 0 & 0 & \bar{Q}_{66} & 0 & 0 \\ 0 & 0 & 0 & \bar{Q}_{55} & 0 \\ 0 & 0 & 0 & 0 & \bar{Q}_{44} \end{bmatrix} \begin{bmatrix} {\varepsilon^c}_{xx} - \alpha_1 \Delta T \\ {\varepsilon^c}_{\theta\theta} - \alpha_2 \Delta T \\ {\varepsilon^c}_{x\theta} \\ {\varepsilon^c}_{xz} \\ {\varepsilon^c}_{\theta z} \end{bmatrix} \tag{10}$$

Noteworthy, the structure is thin enough that the change of stress in the thickness direction can be neglected, and without any external applied stress in this direction, it vanishes. In Eq. (10), The change in temperature is denoted by Δ. The coefficients α_1 and α_2 are thermal expansions in x and θ directions, respectively. Moreover, in Ref. (Ghadiri and Safarpour 2016), the values of stiffness matrix components (Q¯_ij) are presented.

2.4 Kinematic equations of the MEE layer

Using first-order shear deformation shell theory, the

Table 2 Natural frequencies of the shell with m = 1, L/R = 12, and R/h = 50 as they obtained in the present study in comparison with the Ref. (Ke *et al*. 2014a). The dimension of the frequencies are in GHz.

n	Ke *et al* (2014)	Present Study	Error (%)
1	0.7188	0.7079	1.51
2	0.4101	0.4080	0.51
3	0.8003	0.7869	1.67
4	1.4793	1.4663	0.87
5	2.3723	2.3549	0.73
6	3.4695	3.4435	0.74
7	4.7685	4.7291	0.82
8	6.2687	6.2099	0.93
9	7.9694	7.8840	0.11
10	9.8707	9.7497	0.12

kinematic relations for the MEE layer based on are expressed as

$$\begin{aligned} u_M(z,x,t,\theta) &= u_{0M}(x,t,\theta) + z u_{1M}(x,t,\theta) \\ v_M(z,x,t,\theta) &= v_{0M}(x,t,\theta) + z v_{1M}(x,t,\theta) \\ w_M(z,x,t,\theta) &= w_{0M}(x,t,\theta) \end{aligned} \tag{11}$$

Here, displacement variables of the middle surface are axial $u_{0M,}$ circumferential v_{0M} and radial w_{0M} displacements. Two functions u_{1M} and v_{1M} are the rotation functions about axial and circumferential directions, respectively, of the normal vector to the middle plane. Furthermore, the strain tensor components can be obtained as follows (Ebrahimi and Safarpour 2018a, Dai and Safarpour 2021a, Huang *et al*. 2021a, Jiao *et al*. 2021, Moradi *et al*. 2021, Wang *et al*. 2021, Xu *et al*. 2021, Zhang *et al*. 2021a, Zhao *et al*. 2021a)

$$\begin{aligned} \varepsilon^M{}_{xx} &= \frac{\partial u_M}{\partial x} = z\frac{\partial u_{1M}}{\partial x} + \frac{\partial u_{0M}}{\partial x} \\ \varepsilon^M{}_{\theta\theta} &= \frac{1}{R}\frac{\partial v_M}{\partial \theta} + \frac{w_M}{R} = \frac{1}{R}\left(\frac{\partial v_{0M}}{\partial \theta} + z\frac{\partial v_{1M}}{\partial \theta} + w_{0M}\right) \\ \varepsilon^M{}_{xz} &= \frac{1}{2}(u_{1M} + \frac{\partial w_{0M}}{\partial x}) \\ \varepsilon^M{}_{x\theta} &= \frac{1}{2}(\frac{1}{R}\frac{\partial u_{0M}}{\partial \theta} + \frac{\partial v_{0M}}{\partial x}) + \frac{z}{2}(\frac{1}{R}\frac{\partial u_{1M}}{\partial \theta} + \frac{\partial v_{1M}}{\partial x}) \\ \varepsilon^M{}_{\theta z} &= \frac{1}{2}(v_{1M} + \frac{1}{R}\frac{\partial w_M}{\partial \theta} - \frac{v_M}{R}) \end{aligned} \tag{12}$$

2.5 Elasticity equations for MEE layer

The governing elasticity equation in MEE layer are as follows:

$$\sigma_{ij} = c_{ijkl}\varepsilon_{kl} - q_{nij}H_n - e_{mij}E_m - \beta_{ij}\Delta T \tag{13}$$

$$\begin{aligned} D_i &= e_{ikl}\varepsilon_{kl} + d_{in}H_n + s_{im}E_m + p_i\Delta T \\ B_i &= q_{ikl}\varepsilon_{kl} + r_{in}H_n + d_{im}E_m + \lambda_i\Delta T \end{aligned} \tag{14}$$

Models are for the sufficiently thick layer of MEE it is acceptable to use first-order shear deformation theory. Consequently, with this assumption, the strain in z direction in the MEE layer vanishes (Shojaeefard *et al*. 2018). In Eqs. (13) and (14) $c_{ijkl,}$ $s_{im,}$ and $e_{mij,}$ are the elasticity, dielectric, and piezo-electric matrix constants, respectively., D_i and E_m would be electric displacements and electric fields strength, respectively. Moreover, other factors are pertained to the MEE structure's piezo-magnetic properties. The electric, and magnetic field strength, i.e., E_r, E_θ, E_z and H_r, H_θ, H_z where are provided in Eq. (2), may be defined as follow:

$$\begin{aligned} E_x &= -\Phi_{,x}, E_\theta = \frac{-\Phi_{,\theta}}{R+z}, E_z = -\Phi_{,z} \\ H_x &= -\tilde{\vartheta}_{,x}, H_\theta = -\frac{\tilde{\vartheta}_{,\theta}}{R+z}, H_z = -\tilde{\vartheta}_{,z}. \end{aligned} \tag{15}$$

Wang (2002) gave the following relation for the electrical potential

$$\begin{aligned} \Phi(x,\theta,z,t) &= -cos(\beta z)\phi(x,\theta,t) + \frac{2z\phi_0}{h}. \\ \tilde{\vartheta}(x,\theta,z,t) &= -cos(\beta z)\vartheta(x,\theta,t) + \frac{2z\vartheta_0}{h} \end{aligned} \tag{16}$$

in this relation the angle $\beta = \pi/h$ and the variable V_0 and ϑ_0 represent the initial external electric and magnetic potential, respectively.

2.6 Interlamellar compatibility conditions

For the sake of simplicity, the bonding of core nanocomposites to the surrounding MEE layer is considered to be perfect. It means that no relative movement occurs in between the layers. Thus, at thickness coordinate $z = \frac{h_c}{2} = -\frac{h_M}{2}$ the following equations must be satisfied

$$\begin{aligned} u_c &= u_M, \\ v_c &= v_M, \\ w_c &= w_M \\ \text{For } z &= \frac{h_c}{2} = -\frac{h_M}{2} \end{aligned} \tag{17}$$

Imposing these compatibility conditions and using the linear equations in Eq. (9), the following relations can be obtained for the displacement of the neutral surface of the MEE layer (Khalili and Mohammadi 2012, Nasihatgozar and Khalili 2017, Pourmoayed *et al*. 2017):

$$\begin{aligned} u_{0M} &= \frac{\hbar}{2}u_{1M} + u_{0c} + \frac{\hbar}{2}\psi_{1c} \\ v_{0M} &= \frac{\hbar}{2}v_{1M} + v_{0c} + \frac{\hbar}{2}\psi_{1c} \\ w_{0M} &= w_{0c} \end{aligned} \tag{18}$$

2.7 Displacement and boundary equations

According to Hamilton's virtual work principle, displacement and boundary conditions must satisfy the following integral relation (Ma *et al*. 2021, SafarPour and Ghadiri 2017a, SafarPour *et al*. 2017b, c, Hou *et al*. 2021, Huang *et al*. 2021b, Liu *et al*. 2021, Yu *et al*. 2022):

$$\int_{t_1}^{t_2}(-\delta U + \delta W_1 - \delta W_2 + \delta W_3)dt = 0 \tag{19}$$

Moreover, the variation of elastic strain energy of cylindrical shell can be written as (Shariati *et al*. 2012, 2016a, b, 2019, 2020g, 2021a, b):

$$\delta U = \iiint_{V_{core}} (\sigma_{ij}\delta\varepsilon_{ij})\, dV_{core} - \iiint_{V_M} \begin{pmatrix} D_x\delta E_x + D_\theta\delta E_\theta + D_z\delta E_z \\ +B_x\delta H_x + B_\theta\delta H_\theta + B_z\delta H_z \end{pmatrix} dV_M \quad (20)$$

In Eq. (20) σ_{ij} and ε_{ij} are stress and strain tensors components, respectively, which are given in Ref. (Barooti *et al*. 2017). The external work comes from an external electrical load source. There is another energy corresponding to the imposed electric/magnetic load. The variation of this energy is also expressed as follows (Shariati *et al*. 2020a, b, d, g, h)

$$\delta W_1 = \int_{A_M} \left[(N^E + N^M)\left(w_{,x}\delta w_{,x} + v_{,x}\delta v_{,x}\right)\right] dA_M \quad (21)$$

the imposed electric and magnetic loads are denoted by N^E, and N^M which are in the following form (Ke *et al*. 2014b):

$$N^E = -2(e_{31} - \frac{c_{13}e_{33}}{c_{33}})\phi_0$$
$$N^M = -2(\beta_{31} - \frac{c_{13}\beta_{33}}{c_{33}})\psi_0 \quad (22)$$

Here a non-uniform temperature is assumed in the thickness of the shell in thermal environment conditions. Thus, the corresponding work of temperature gradient can be obtained as:

$$\delta W_2 = \iint_{A_c} \begin{bmatrix} (N_1^T)(\frac{\partial w_{0c}}{\partial x}\frac{\partial\delta w_{0c}}{\partial x}) \\ +(N_2^T)(\frac{\partial v_{0c}}{\partial x}\frac{\partial\delta v_{0c}}{\partial x}) \end{bmatrix} R dx d\theta \quad (23)$$

The thermal resultants, N_1^T and N_2^T, are obtained as follows:

$$N_1^T = \int_{-\hbar_c/2}^{\hbar_c/2} (\bar{Q}_{11} + \bar{Q}_{12})\alpha(T - T_0) dz_c,$$
$$N_2^T = \int_{-\hbar_c/2}^{\hbar_c/2} (\bar{Q}_{21} + \bar{Q}_{22})\alpha(T - T_0) dz_c. \quad (24a)$$

The vector α includes the coefficients of thermal expansion:

$$\alpha = [\alpha_1\alpha_2 000]^T \quad (24b)$$

Also, the MEE layer is covered by elastic foundation. The work done due to this foundation is as follows:

$$\delta W_3 = \iint_{A_M} [(K_w)w_M\delta w_M]\, R dx d\theta \quad (25)$$

Assuming a linear change for temperature in thickness of the shell from T_m at the outer surface toT_c at the inner surface and substituting Eqs. (20)-(25) into Eq. (19), after solving the obtained equation, variation of displacement components in core and MEE layer can be acquired.

$$\delta u_c: N^c{}_{xx,x} + \frac{N^c{}_{x\theta,\theta}}{R} = 0, \quad (26)$$

Table 3 The dimensionless natural frequency calculated using the formulation in the present study in comparison with the corresponding values presented in Ref. (Liu *et al*. 2018)

$m\pi L/l_{GNP}$	Epoxy Ref	Epoxy Present	GNP-UD Ref (Liu *et al*. 2018)	GNP-UD Present
2	0.9659	0.93659	2.3674	2.3036
5	2.6997	2.66985	6.6185	6.4865
10	5.6503	5.62659	13.8540	13.8075

$$\delta v_c: N^c{}_{x\theta,x} + \frac{N^c{}_{\theta\theta,\theta}}{R} + \frac{Q^c{}_{z\theta}}{R} - (N_1^T)v_{0,x^2} = 0 \quad (27)$$

$$\delta w_c: Q^c{}_{xz,x} + \frac{Q^c{}_{z\theta,\theta}}{R} - \frac{N^c{}_{\theta\theta}}{R} - (N_1^T)w_{0c,x^2} = 0, \quad (28)$$

$$\delta\psi^c{}_x: M^c{}_{xx,x} + \frac{M^c{}_{\theta\theta,\theta}}{R} - Q^c{}_{xz} = 0, \quad (29)$$

$$\delta\psi^c{}_\theta: \frac{M^c{}_{\theta\theta,\theta}}{R} + M^c{}_{x\theta,x} - Q^c{}_{z\theta} = 0. \quad (30)$$

$$\delta u_0^M: \frac{\partial N^M{}_{xx}}{\partial x} + \frac{1}{R}\frac{\partial N^M{}_{x\theta}}{\partial\theta} + X_{31}\phi_{,x} + X_{32}\vartheta_{,x} = 0 \quad (31)$$

$$\delta v_0^M: \frac{\partial N^M{}_{x\theta}}{\partial x} + \frac{1}{R}\frac{\partial}{\partial\theta}N^M{}_{\theta\theta} + \frac{Q^M{}_{z\theta}}{R} + \frac{X_{61}}{R}\phi_{,\theta} - \frac{k_sX_{24}}{R}\phi_{,\theta} + \frac{Y_{61}}{R}\vartheta_{,\theta} - \frac{k_sY_{24}}{R}\vartheta_{,\theta} - (N^E + N^M)v_{0p,x^2} = 0 \quad (32)$$

$$\delta w_0^M: \frac{\partial Q^M{}_{xz}}{\partial x} + \frac{1}{R}\frac{\partial Q^M{}_{z\theta}}{\partial\theta} - \frac{N^M{}_{\theta\theta}}{R} - \frac{k_sX_{24}}{R}\phi_{,\theta^2} - k_sX_{15}\phi_{,x^2} - \frac{k_sY_{61}}{R}\vartheta_{,\theta^2} - k_sY_{15}\vartheta_{,x^2} - (N^E + N^M)w_{0M,x^2} - K_w w_M = 0, \quad (33)$$

$$\delta u_1^M: \frac{\partial M^M{}_{xx}}{\partial x} + \frac{1}{R}\frac{\partial M^M{}_{\theta\theta}}{\partial\theta} - Q^M{}_{xz} + X_{32}\phi_{,x} + k_sX_{12}\phi_{,x} + X_{35}\vartheta_{,x} + k_sX_{21}\vartheta_{,x} = 0, \quad (34)$$

$$\delta v_1^M: \frac{1}{R}\frac{\partial M^M{}_{\theta\theta}}{\partial\theta} + \frac{\partial M^M{}_{x\theta}}{\partial x} - Q^M{}_{z\theta} + \frac{X_{62}}{R}\phi_{,\theta} + k_sX_{13}\phi_{,\theta} + \frac{X_{64}}{R}\vartheta_{,\theta} + k_sX_{23}\vartheta_{,\theta} = 0 \quad (35)$$

The displacement equation of MEE layer can be expressed as follows:

$$\delta\phi = \int_{-\hbar_M/2}^{\hbar_M/2} \left\{ \begin{matrix} cos(\beta z)\left[D_x\delta\phi_{,x} + \frac{D_\theta}{R+z}\delta\phi_{,\theta}\right] \\ +D_z\beta\, sin(\beta z)\delta\phi \end{matrix} \right\} dz = 0$$
$$\delta\vartheta = \int_{-\hbar_M/2}^{\hbar_M/2} \left\{ \begin{matrix} cos(\beta z)\left[B_x\vartheta_{,x} + \frac{B_\theta}{R+z}\vartheta_{,\theta}\right] \\ +B_z\beta\, sin(\beta z)\delta\vartheta \end{matrix} \right\} dz = 0 \quad (36)$$

For the above Eqs. (26)-(36), the following assumption have been made:

$$(N^i{}_{xx}, N^i{}_{x\theta}, N^i{}_{\theta\theta}) = \int_{-h_i/2}^{h_i/2} (\sigma^i{}_{xx}, \sigma^i{}_{x\theta}, \sigma^i{}_{\theta\theta}) dz, i = c, M$$
$$(M^i{}_{xx}, M^i{}_{x\theta}, M^i{}_{\theta\theta}) = \int_{-h_i/2}^{h_i/2} (\sigma^i{}_{xx}, \sigma^i{}_{x\theta}, \sigma^i{}_{\theta\theta}) z dz\,, i = c, M \quad (37)$$

$$(Q^{i}_{xz}, Q^{i}_{z\theta}) = \int_{-h_i/2}^{h_i/2} k_s(\sigma^{i}_{xz}, \sigma^{i}_{z\theta})dz\,, i = c, M$$

In the above relations, some parameters are used, which can be obtained using the following two equations:

$$\begin{aligned}
&\int_{-\frac{h_M}{2}}^{\frac{h_M}{2}} D_x\, cos(\beta z) = X_{11}\frac{\partial \phi}{\partial x} + Y_{11}\frac{\partial \vartheta}{\partial x} + X_{12}\left(u_{1M} + \frac{\partial w_{0M}}{\partial x}\right),\\
&\int_{-\frac{h_M}{2}}^{\frac{h_M}{2}} D_\theta \frac{cos(\beta z)}{R_M + z} = X_{22}\frac{\partial \phi}{\partial \theta} + Y_{22}\frac{\partial \vartheta}{\partial \theta}\\
&+X_{13}\left(v_{1M} + \frac{1}{R}\frac{\partial w_{0M}}{\partial \theta} - \frac{v_{0M}}{R}\right),\\
&\int_{-\frac{h_M}{2}}^{\frac{h_M}{2}} D_z \beta\, sin(\beta z)\\
&= -X_{33}\phi - Y_{33}\vartheta + X_{31}\left(\frac{\partial u_{0M}}{\partial x}\right) + X_{32}\left(\frac{\partial u_{1M}}{\partial x}\right)\\
&+X_{61}\left(\frac{1}{R}\frac{\partial v_{0M}}{\partial \theta} + \frac{w_{0M}}{R}\right) + X_{62}\left(\frac{1}{R}\frac{\partial v_{1M}}{\partial \theta}\right),\\
&\int_{-\frac{h_M}{2}}^{\frac{h_M}{2}} B_x\, cos(\beta z) = Y_{11}\frac{\partial \phi}{\partial x} + T_{11}\frac{\partial \vartheta}{\partial x} + X_{21}\left(u_{1M} + \frac{\partial w_{0M}}{\partial x}\right),\\
&\int_{-\frac{h_M}{2}}^{\frac{h_M}{2}} B_\theta \frac{cos(\beta z)}{R + z} = Y_{22}\frac{\partial \phi}{\partial \theta} + T_{22}\frac{\partial \vartheta}{\partial \theta}\\
&+X_{23}\left(v_{1M} + \frac{1}{R}\frac{\partial w_{0M}}{\partial \theta} - \frac{v_{0M}}{R}\right),\\
&\int_{-\frac{h_M}{2}}^{\frac{h_M}{2}} B_z \beta\, sin(\beta z) = -Y_{33}\phi - T_{33}\vartheta + X_{34}\left(\frac{\partial u_{0M}}{\partial x}\right)\\
&+X_{35}\left(\frac{\partial u_{1M}}{\partial x}\right) + X_{63}\left(\frac{1}{R}\frac{\partial v_{0M}}{\partial \theta} + \frac{w_{0M}}{R}\right) + X_{64}\left(\frac{1}{R}\frac{\partial v_{1M}}{\partial y}\right).
\end{aligned} \tag{38}$$

where:

$$\begin{aligned}
&\{X_{11}, Y_{11}\} = \int_{-h/2}^{h/2} \{s_{11e}, d_{11e}\}(\cos(\beta z))^2 dz,\\
&\{X_{22}, Y_{22}\} = \int_{-h/2}^{h/2} \{s_{22e}, d_{22e}\}\left(\frac{\cos(\beta z)}{R + z}\right)^2 dz,\\
&T_{11} = \int_{-h/2}^{h/2} r_{11e}(\cos(\beta z))^2 dz,\\
&T_{22} = \int_{-h/2}^{h/2} r_{22e}\left(\frac{\cos(\beta z)}{R + z}\right)^2 dz\\
&X_{11} = \int_{-\hbar p/2}^{\hbar p/2} \{s_{11e}\}\, cos^2(\beta z)\, dz,\\
&X_{22} = \int_{-\hbar p/2}^{\hbar p/2} \{s_{22e}\}\frac{cos^2(\beta z)}{(R_p + z)^2} dz,\\
&X_{13} = \int_{-\hbar p/2}^{\hbar p/2} \frac{cos(\beta z)}{R + z} e_{24e} dz,\\
&X_{33} = \int_{-\hbar p/2}^{\hbar p/2} \{s_{33e}\}\beta^2\, sin^2(\beta z)\, dz,\\
&X_{3i} = \int_{-\hbar p/2}^{\hbar p/2} \{1, z_p\}\beta e_{31e}\, sin(\beta z)\, dz,\\
&X_{6i} = \int_{-\hbar p/2}^{\hbar p/2} \{1, z\}\beta e_{32e}\, sin(\beta z)\, dz.
\end{aligned} \tag{39}$$

Noteworthy, using all these relations and imposed compatibility conditions, the number of unknown in these equations reduces by the number of 3 from 12 unknowns to 9 unknowns. For solving these equations, boundary conditions are also necessary. In the following for different boundary scenarios in terms of displacement are given.

Shell with clamped ends conditions at $x = 0,\ L$:

$$\begin{aligned}
&u_{0c} = v_{0c} = w_{0c} = 0,\\
&\psi^c_x = \psi^c_\theta = 0,\\
&u_{0M} = v_{0M} = w_{0M} = 0,\\
&u_{1M} = v_{1M} = 0,\\
&\phi = \vartheta = 0
\end{aligned} \tag{40}$$

Shell with simply supported ends at $\theta = \pi/2,\ 3\pi/2$

$$\begin{aligned}
&u_{0c} = w_{0c} = u_{0M} = w_{0M} = 0,\\
&\psi^c_x = u_{1p} = 0, \phi = \vartheta = 0\\
&v_{0c} \neq 0, \psi^c_\theta \neq 0,\\
&v_{0M} \neq 0, v_{1M} \neq 0.
\end{aligned} \tag{41}$$

3. Solution strategy

For numerically solving the equations, the differential quadrature method (DQM) is utilized (Adamian *et al*. 2020, Al-Furjan *et al*. 2020f, g, Li *et al*. 2020, Shi *et al*. 2020, Zare *et al*. 2020, Dai *et al*. 2021b, Zhang *et al*. 2021a). This method, compared to others, has a high convergence rate and accuracy and was introduced by Bellman *et al*. (Bellman *et al*. 1972). In this method, the number of seeds is the main parameter that affect the accuracy of results. However, the computational cost increases significantly with excessive seeds. On the other hand, using few seeds lead to non-accurate results. Thus, a compromise between computational cost and number of seeds is recommended (Bellman and Casti 1971, Bellman *et al*. 1972). In the very first versions of this method, limitation in selecting the number of seeds was an issue to reach the desired accuracy. Shu (2012) improved this method by using an infinite number of seeds. Shu and Richards (1992) used this method in multi-domain equations by decomposing the domain into separate domains. In the present study, the GDQ method is utilized to solve the obtained equations in the previous section. For this aim, the approximate r-th derivative of $f(x)$ is obtained by decomposing the derivative to a set of the linear combination values of the function (Rajasekaran 2009):

$$\left.\frac{\partial^r f(x)}{\partial x^r}\right|_{x=x_p} = \sum_{j=1}^{n} C^{(r)}_{ij} f(x_i) \tag{42}$$

In this relation, n is the total number of seeds used in x-coordinate direction, and C_{ij} is the weighting coefficients. The weighting coefficients for the first derivative can be calculated using the following equation:

$$\begin{aligned}
C^{(1)}_{ij} &= \frac{M(x_i)}{M(x_j)} \times \frac{1}{(x_i - x_j)}\\
for\ i \neq j \quad &\text{and } i, j = 1,2,\ldots,n\\
C^{(1)}_{ij} &= \sum_{i \neq j, j=1}^{n} -C^{(1)}_{ij} \quad for i = j
\end{aligned} \tag{43}$$

where

$$M(x_p) = \prod_{p\neq q, q=1}^{n} (x_p - x_q) \tag{44}$$

For higher derivatives, the weighting coefficients are calculated using the first derivative coefficients:

$$\begin{aligned} &C_{ij}^{(r)} = r\left[C_{ij}^{(r-1)}\left[C_{ij}^{(1)} - \frac{1}{(x_i - x_j)}\right]\right] \\ &\text{for } i \neq j, 2 \leq r \leq n-1, \text{and } i,j = 1,2,\ldots,n \\ &C_{ii}^{(r)} = -\sum_{i\neq j, j=1}^{n} C_{ij}^{(r)} \\ &\text{for } 1 \leq r \leq n-1 \text{ and } i,j = 1,2,\ldots,n \end{aligned} \tag{45}$$

The seeds in generated in a non-uniform pattern on the neutral surface of the cylindrical shell as a function of coordinates on the surface, i.e., x and θ:

$$\begin{aligned} &x_i = \frac{L}{2}(1 - cos\,\gamma), \gamma = \pi\frac{i-1}{N_i - 1} \\ &fori = 1,2,3,\ldots,N_i \end{aligned} \tag{46}$$

Thus, the displacement components and normal functions can be assumed to be harmonic:

$$\begin{aligned} &u_{0i}(x,\theta,t) = U_{0i}(x)\,cos(m\theta) fori = c,p \\ &v_{0i}(x,\theta,t) = V_{0i}(x)\,sin(m\theta), fori = c,p \\ &w_{0i}(x,\theta,t) = W_{0i}(x)\,cos(m\theta), fori = c,p \\ &\psi^{c}{}_{x}(x,\theta,t) = \Psi^{c}{}_{x}(x)\,cos(m\theta), \\ &\psi^{c}{}_{\theta}(x,\theta,t) = \Psi^{c}{}_{\theta}(x)\,sin(m\theta), \\ &u_{1M}(x,\theta,t) = U_{1M}(x)\,cos(m\theta), \\ &v_{1M}(x,\theta,t) = V_{1M}(x)\,sin(m\theta), \\ &\phi(x,\theta,t) = \varphi(x)\,cos(m\theta), \\ &\vartheta(x,\theta,t) = \varsigma(x)\,cos(m\theta). \end{aligned} \tag{47}$$

Rearranging the quadrature analogs of field equations and boundary conditions inside the fabric of a generalized eigenvalue problem yields:

$$\left\{\begin{bmatrix}[F_{ad}] & [F_{ab}] \\ [F_{bd}] & [F_{bb}]\end{bmatrix} N_{cr} + \begin{bmatrix}[K_{ad}] & [K_{db}] \\ [K_{bd}] & [K_{bb}]\end{bmatrix}\right\}\begin{Bmatrix}\delta_d \\ \delta_b\end{Bmatrix} = 0 \tag{48}$$

where the subscripts d and b stands for the domain and boundary grid points, respectively. Furthermore, δ is the displacement vector. Eq. (48) is transformed to a standard eigenvalue problem as follows:

$$\begin{aligned} &[K^*]\{\delta_i\} = (N_{Cr})[F^*]\{\delta_i\} \\ &[K^*] = [K_{dd} - K_{db}{K_{bb}}^{-1}K_{bd}] \\ &[F^*] = [F_{dd} - F_{db}{K_{bb}}^{-1}K_{bd}] \end{aligned} \tag{49}$$

Critical temperature and voltage of the sandwich structure are obtained when these equations vanish. Finally, a dimensionless parameter is defined according to Ref. (Ke *et al*. 2014):

$$\begin{aligned} &\Phi^* = \frac{100 \times \phi}{\sqrt{A_{11}/X_{33}}} \\ &\Delta T^* = \Delta T \times \alpha \end{aligned} \tag{50}$$

4. Numerical results

The developed equations of GNP nanocomposites shell coupled with MEE layer in the thermal environment is now solved for various models with different boundary conditions. First, the structure is modeled, then the effects of MEE layer, temperature change, and pattern of dispersion of GNP on critical voltage and critical temperature are evaluated. In the following sections, it is demonstrated that the mentioned parameters have a considerable influence on the static response of the composite structures, which are electrically actuated.

Table 4 The calculated natural frequency in the present study as a function of applied voltage compared to the corresponding values given in Ref. (Ghadiri and Safarpour 2016)

ϕ_o [V]	Ref. (Ghadiri and Safarpour 2016)	Present study
-0.02	0.03030	0.03030
-0.015	0.03012	0.03017
-0.01	0.03004	0.03004
-0.005	0.02991	0.02991
0	0.02978	0.02978
0.005	0.02960	0.02964
0.01	0.02951	0.02951
0.015	0.02938	0.02938
0.02	0.02925	0.02925

4.1 Convergence

The convergence of the results is guaranteed with a sufficient number of the grid. For various boundary conditions and materials, convergence studies are conducted. As can be seen in Table 1, convergence is achieved when at least nine grid points are used. In addition, in the structure with simply-simply boundary conditions, a smaller critical temperature is seen, wherein the structure with the clamped-clamped ones would be stiffer than the others. Moreover, the addition of GNP reinforcing nanofillers leads to the GNPRC cylindrical shell has a higher critical temperature compared to pure epoxy.

5. Comparative study based on deep learning

In recent years, deep learning has attracted many interests as an applicable tool in a wide range of fields, including regression, classification and segmentation duties. Thereby, a deep neural network (DNN) is created here with optimized factors obtained by ADADELTA (an abbreviation for adaptive delta). The set of $X = \left\{\frac{h_M}{h}, B.Cs, g_{GPL}\right\}^T$ has been selected as the input of regression-based DNN to estimate the critical conditions. In Fig. 2 the schematic of the created DNN is demonstrated. DNN's each layer has numerical units called perceptron. The next figure (Fig. 3) illustrates the details of operations conducted in a single perceptron. The perceptron input would be the output of the units constituting the last network layer. To achieve the numerical unit output, the amount of each input should be

Table 5 Material constants of the GNP and epoxy as provided in Ref. (Wu *et al*. 2017)

Constants	Epoxy	GNP
Young's modulus (GPa)	3	1010
Poisson's ratio	0.34	0.186
Thermal expansion coefficient(10^{-6}/K)	60	5
Density (kg m^{-3})	1200	1062.5

Table 6 Material constants of the MEE layer

Material constants	$BiTiO_3 - CoFe_2O_4$
Elastic (GPa)	$c_{11} = 226, c_{12} = 125, c_{13} = 124, c_{33} = 216, c_{44} = 44.2, c_{55} = 44.2, c_{66} = 50.5$
Mass density (10^3kg m^{-3})	$\rho = 5.55$
Piezomagnetic (N A m^{-1})	$q_{15} = 275, q_{31} = 290.1, q_{33} = 349.9$
Magnetoelectric (10^{-12}Ns VC^{-1})	$d_{11} = 5.367, d_{33} = 2737.5$
Magnetic (10^{-6} Ns^2 C^{-2})	$r_{11} = -297, r_{33} = 83.5$
Piezoelectric(C m^{-2})	$e_{31} = -2.2, e_{33} = 9.3, e_{15} = 5.8$
Dielectric (10^{-9} C V m^{-1})	$s_{11} = 5.64, s_{22} = 5.64, s_{33} = 6.35$
Thermal moduli (10^5 N Km^{-2})	$\beta_1 = 4.74, \beta_3 = 4.53$
Pyroelectric (10^{-6} C N^{-1})	$P_3 = 25$
Pyromagnetic (10^{-6} N Am K^{-1})	$\lambda_3 = 5.19$

mathematically operated with biases and weights. For gaining more information regarding the fundamentals of the neural network method, readers are referred to the (White 1992). The mean squared error (MSE) would be the metric chosen in this research to examine the DNN accuracy in critical conditions' prediction. Next relation explains MSE as the squared discrepancy's mean between the predicted critical conditions and expected one.

$$\text{MSE}=\frac{1}{n}\sum_{\text{i=1}}^{n}\left(\text{Y-}\hat{\text{Y}}\right)^{2}. \tag{51}$$

5.1 ADADELTA optimizer to tune the DNN factors

ADADELTA has been selected as an optimizer for finding suitable biases and weights in order to reduce the MSE. The key benefit of ADADELTA is listed as follows:

• This technique would set the rate of learning automatically

• ADADELTA would not sensitive to the amounts of the hyperparameters

• This technique has the ability to be employed in local conditions along with the distributed one

The next relation is applied at all iteration steps (epoch) to update the neural network factors (weights and biases):

$$\hbar_{t+1} = \hbar_t + \triangle \hbar_t \triangle \chi_t = -\eta \frac{\partial f(\chi_t)}{\partial \chi_t} \tag{52}$$

here, η implies the primary learning rate. For simplifying the gradient of the involved factors at the t[th] epoch, we applied G_t in form of $\frac{\partial f(\hbar_t)}{\partial \hbar_t}$. To achieve the weights and biases updates, it would be needed to compute the gradient root mean square at the provided epoch by next equation

$$RMS[\Re_t] = \sqrt{E\left[\Re_t^2\right] + \varepsilon} \tag{53}$$

here, ε would be a constant. It could be implied that $E\left[\Re_t^2\right]$ illustrates the expected amount of the squared gradient, which may be achieved based on the subsequent definition

$$E\left[\Re_t^2[]\, E\left[\Re_{t-1}^2[](1-\rho)_t^2\right]\right] \tag{54}$$

then, ρ implies to the decay rate. Employing Eq. (53) and Eq. (54), one would achieve the update of the mentioned factors as follow

$$\triangle \hbar \frac{\eta}{RMS[\Re_t[]]_{t_t}} \tag{55}$$

To demonstrate the ADADELTA performance in comparison with other optimizers, Zeiler (2012) investigated their error in dividing the handwriting MNIST digits dataset for 50 epochs. As shown, ADADELTA performs satisfactorily compared to the other optimization techniques and reaches the final amount the error for the lowest number. Thus, ADADELTA can be recognized as one of the high-speed optimization techniques with the ability to reach the lower amount of the least error amongst the well-known optimizers. As already shown, ADADELTA technique had been used to adjust the factors of DNN to create a regression-based estimator of disk's vibration response. The hidden layers' activation function would act based on Rectified linear unit (ReLU). The procedure of training would be conducted by applying the 70% of the dataset. The results' accuracy would be examined by investigating the MSE of the validation and testing step of dataset.

5.2 Model validation

In Table 2, a comparative study of the results of the current paper and those of the literature is presented. A satisfactory agreement can be seen between the dimensionless natural frequency of the current study and Ref. (Ke *et al*. 2014). According to the data given in the table, the natural frequency increases with increasing the wave number (n). As another verification, in Table 3, the natural frequency of simply supported cylindrical shell in comparison with the corresponding values presented in Ref. (Liu *et al*. 2018). One more verification is conducted for this work. In Table 4, consistency between values calculated for the frequency with the results of Ref. (Ghadiri and Safarpour 2016) demonstrates the capability of this model (MEE cylindrical shell) in providing reasonable results. Furthermore, the natural frequency decreases with increasing the applied voltage. The reason for such behavior could be explained as follows: employing the positive (or negative) electric voltages causes circumferential and axial tensile (or compressive) forces, respectively. As can be seen,

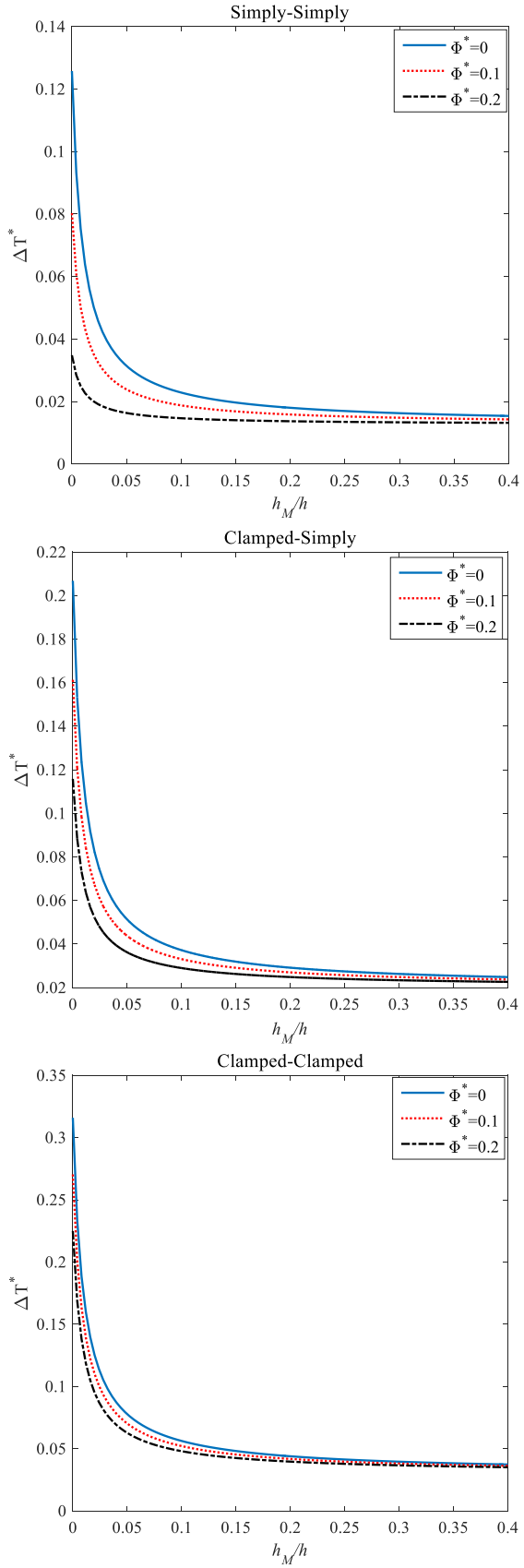

Fig. 4 Calculated critical temperature as a function of the inverse thickness of MEE layer (horizontal axis) at different values of applied external voltage for clamped-clamped supported GNPRC structure coupled with MEE layer with L/R = 10, R/h = 10, ϑ = 1(A) and Pattern 4

there is a good agreement between the results of the current study and other published articles.

5.3 Parametric study

Semi-numerical results are presented in this section for GNP cylindrical shell covered with MEE layer. Throughout this article, the geometrical parameters of the GNP structure are length a_{GNP} = 2.5μm, thickness h_{GNP} = 1.5nm, and radius R_{GNP} = 0.75μm. Table 5 also includes the material constants of the GNP. The properties of PMMA material which is considered as the matrix of nanocomposites under study here are dependent on temperature. The thermal expansion coefficient for this material as a function of temperature is given by relation $\alpha_m = 45(1 + 0.0005\Delta T) \times 10^{-6}/K$. Moreover, the elasticity modulus is also significantly affected by temperature, and it cannot be neglected. The dependency of elasticity modulus on temperature is approximated by $E = (3.52 - 0.0034T)\,GPa$, in which $T = T_0 + \Delta T$. Furthermore, in Table 6 the material constants of the MEE layer are given. Now, the dependency of critical temperature and voltage on the different parameters is evaluated.

5.4 Applied voltage and MEE thickness effects on the critical temperature

Correlations between the critical temperature and MEE thickness are presented in Figs. 4 for several scenarios of boundary conditions and external applied voltage with *L/R = 10* and g_{GPL} *= 1%*. As seen in these graphs, the critical temperature of the structure increases with a decrease in the MEE thickness. One explanation is that increasing the external applied voltage, the negative and positive electric potentials, circumferential and axial tensile, and compressive forces are generated leads to reduction of the critical temperature and stability of the structure. This increase in critical temperature is more significant for clamp-clamp boundary conditions. Improving the stability of the structure with boundary conditions change from simply-simply to clamped-clamped, in Fig. 4, results in raising the critical temperature.

5.5 Influence of GNP weight fraction and applied voltage on critical temperature

Fig. 5 illustrates the variation of critical temperature versus the GNP weight fraction for different boundary conditions and applied voltages with h/h_M *= 10* and *h = R/10*. The results are given for three different boundary conditions. A common behavior is that with increasing the GNP weight fraction, the critical temperature increases significantly in the lower GNP weight fraction for all boundary conditions, and the effects decrease in the higher values GNP weight fraction. The increasing of critical temperature with GNP weight fraction is remarkable for clamped-clamped B.Cs. On the other hand, increasing the external applied voltage results in critical temperature decreases. This change is more apparent in the low GNP weight fraction.

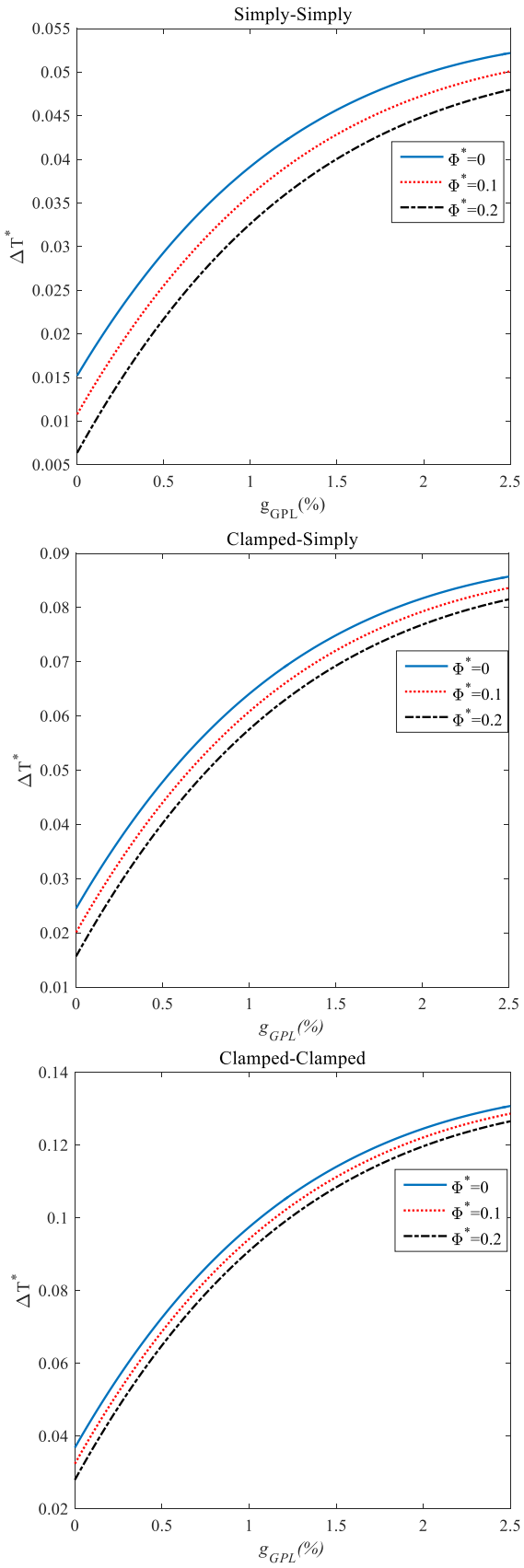

Fig. 5 Calculated critical temperature as a function of g_GNP (horizontal axis) at different values of applied external voltage for clamped-clamped supported GNPRC structure coupled with MEE layer for L/R = 10, R/h = 10, ϑ = 1(A) and Pattern 4

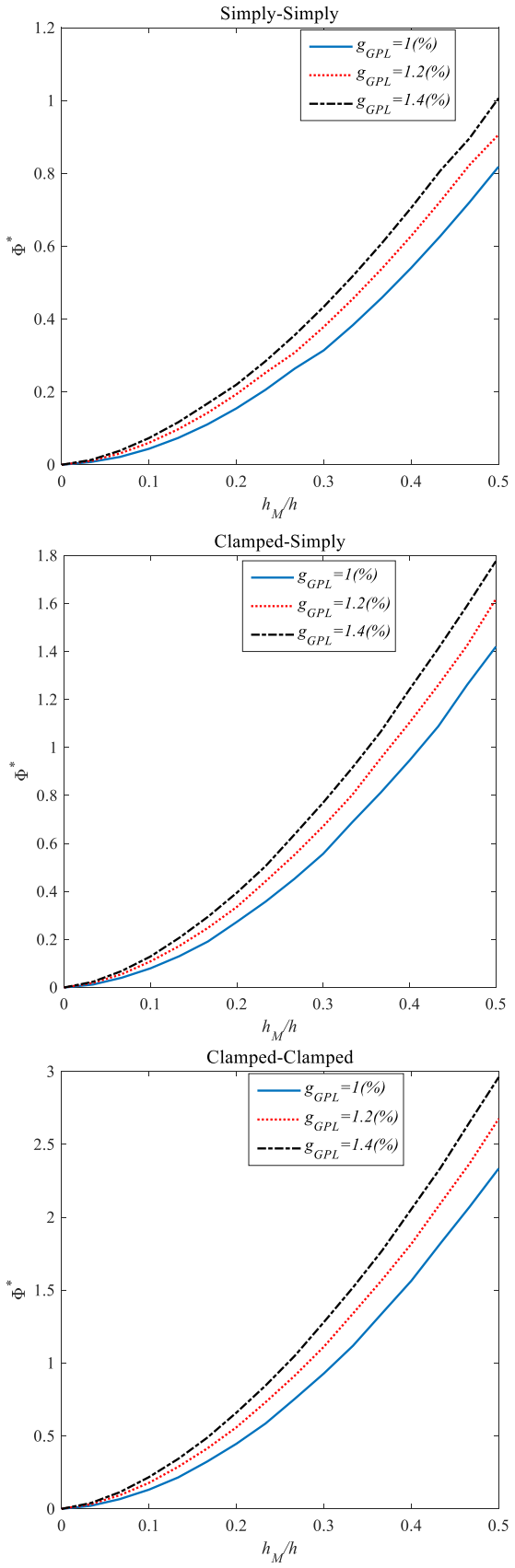

Fig. 6 Calculated critical temperature as a function of g_GNP (horizontal axis) at different values of applied external voltage for clamped clamped supported GNPRC structure coupled with MEE layer for L/R = 10, R/h = 10, ϑ = 1(A) and Pattern 4

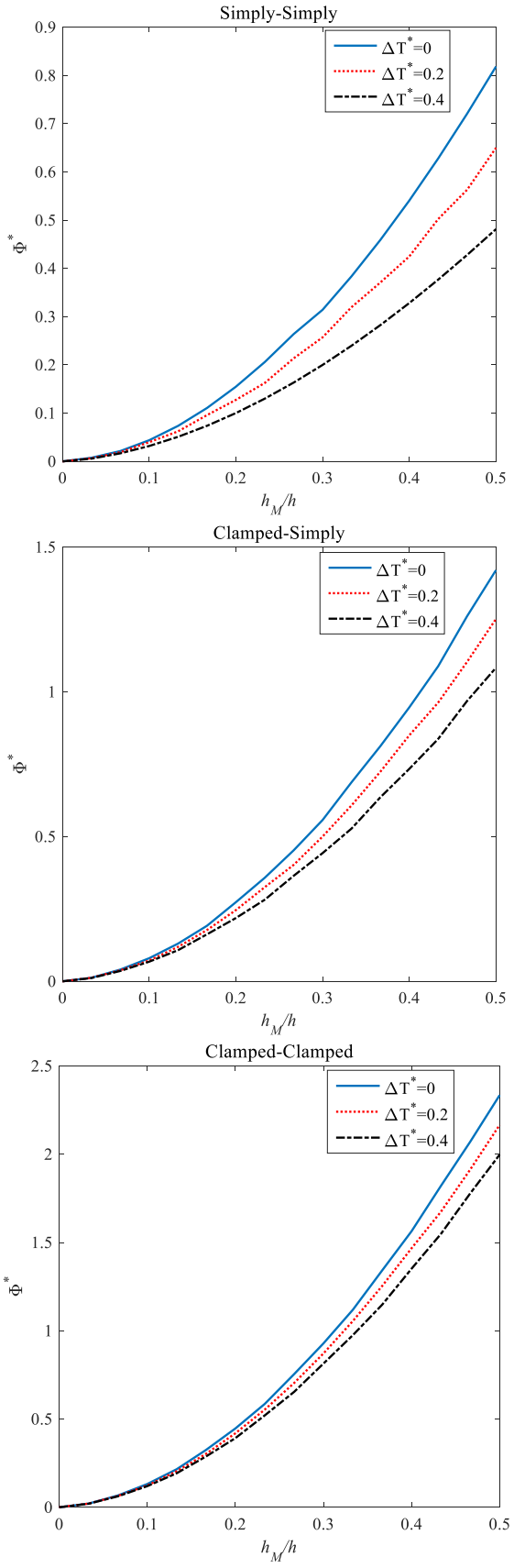

Fig. 7 Calculated dimensionless critical voltage as a function of hM/h and non-dimensional temperature changes for clamped-clamped supported GNPRC structure coupled with MEE layer for L/R = 10, R/h = 10, ϑ = 1(A) and Pattern 4

5.6 GNP weight fraction and MEE thickness effects on the critical voltage

Dependency of the critical voltage on the thickness of MEE layer (h_M) for different weight fraction of GNP and B. Cs are presented in Fig. 6. It is clear that the shell's critical voltage is associated to the value of h_M/h. Indeed, a significant and smooth increase in the critical voltage is evident with increasing h_M/h. Furthermore, the amount of increase in the critical voltage is more pronounce at certain values of h_M/h ($0.3 < h_M/h$). On the other hand, the critical voltage of the cylindrical shell increases with increasing the GNP weight fraction. By comparing Fig. 6, it can be deduced that both the stability and external voltage decrease whenever the end condition of the shell changes from simply supported to clamped ends.

Fig. 7 illustrate the variation of dimensionless critical voltage versus the non-dimensional temperature changes for different boundary conditions with $h/h_M = 10$ and $h = R/10$. The results are given for three different boundary conditions. A common behavior is that by increasing the non-dimensional temperature changes, the dimensionless critical voltage decreases significantly. The increasing of critical voltage with increase/decrease temperature changes is remarkable for clamped-clamped B.Cs. On the other hand, increasing the temperature change results in critical voltage decreases. This change is more apparent in the higher values of h_M/h.

5.7 Comparing DNN outcomes with results of current study

For comparing the ADADELTA performance with another optimizer, Zeiler (2012) investigated their errors in classifying the handwriting MNIST dataset digits for 50 epochs. As the aforementioned figure demonstrated, ADADELTA performance exceeds other optimization techniques and reaches the final amount of the error during the least number. Then, ADADELTA would be classified as one of the extremely fast optimizers which would be able to reach fewer amounts of the least error amongst well-known optimization techniques. As it is previously mentioned, ADADELTA approach has been applied to tune the factors of DNN to create a regression-based estimator of vibrations of a disk. The hidden layers' activation function acts due to the Rectified linear unit (ReLU). The procedure of training has been conducted by employing 70% of the dataset. The results' accuracy has been evaluated by investigating the MSE of the validation and testing part of the dataset. The training procedure's outcomes have been shown in Table 7. According to this table, the nuance between the predicted dimensionless critical temperature and the expected ones would be totally desirable. It would be due to the fact that there are very small distances between the predicted points from the fitting line. The training procedure's small MSE ($MSE_{Train} = 2 * 10^{-6}$) implies the superb ability of ADADELTA for finding the suitable factors to tune the DNN. To make the mentioned performance of the mentioned fully connected DNN reliable, it would be needed to analyze the approach's accuracy toward verified and test sets. Also, according to this table, it would be due

Table 7 DNN's estimation performance of the model with respect to training data with L/R = 10, R/h = 10, g_GNP = 1% ϑ = 1(A) and Pattern 4

$\frac{h_c}{h_M} = 10$				
		Predicted		
Φ^*	Fit	$MSE_{Train} = 1.2 \times 10^{-6}$	$MSE_{Train} = 1.6 \times 10^{-6}$	$MSE_{Train} = 2 \times 10^{-6}$
0.02	0.2061	0.2525	0.2132	0.2085
0.04	0.2186	0.1673	0.2012	0.2123
0.06	0.2303	0.1821	0.2142	0.2291
0.08	0.2424	0.3175	0.2546	0.2473
0.1	0.2545	0.1923	0.2452	0.2512
0.12	0.2666	0.2894	0.2723	0.2673
0.14	0.2787	0.2154	0.2652	0.2745
0.16	0.2908	0.3721	0.3012	0.2991
$\frac{h_C}{h_M} = 50$				
0.02	0.1691	0.0985	0.1541	0.1612
0.04	0.1782	0.2121	0.1875	0.1799
0.06	0.1878	0.2212	0.1963	0.1901
0.08	0.1962	0.1432	0.1863	0.1941
0.1	0.1057	0.2512	0.2112	0.2061
0.12	0.2145	0.2011	0.2095	0.2101
0.14	0.2241	0.2921	0.2345	0.2291
0.16	0.2332	0.2541	0.2412	0.2341

to the fact that there are very small distances in estimated points from the fitting line. The small MSE of the test procedure ($MSE_{Test} = 1.2 * 10^{-6}$) illustrates the strength of the mentioned technique to estimate the dimensionless temperature change of the system.

6. Conclusions

The thermo-electrical characteristics of GNPRC shell coupled with MEE layer were evaluated. In this regard, a cylindrical smart nanocomposite made of GNPRC coupled with MEE layer was considered. Because of the layer nature of the structure, the material characteristics of the whole structure were regarded as graded. Both mechanical and thermal boundary conditions were applied to this structure. The main objective of this work was to determine critical temperature and critical voltage as a function of thermal condition, support type, GNP weight fraction, and MEE thickness. The governing equation of the multilayer nanocomposites cylindrical shell was derived. The GDQM was employed to numerically solve the differential equations. This method was integrated with DNN with ADADELTA optimizer to determine the critical voltage and temperature change of the structure. The outcome of this study indicated that:

• The critical temperature and voltage decrease with decreasing in the MEE thickness. These decreases in not uniform. Up to some critical point in the thickness of the MEE layer, the change in critical temperature and voltage are more pronounce.

• Generally, clamped end structures show more stable behavior. As the ends changed from clamped to simply supported, both critical temperature and voltage decrease significantly.

• The critical temperature decrease with an increase in applied external voltage. The change in critical temperature is more obvious in thinner MEE layer, lower.

• The critical voltage increase with an increase in GNP' weight fraction. The change in critical voltage is more obvious in thinner MEE layer.

• The small MSE of the test procedure illustrates the strength of the mentioned technique to estimate the dimensionless temperature change of the system

Acknowledgments

The Deanship of Scientific Research (DSR) at King Abdulaziz University, Jeddah, Saudi Arabia has funded this project, under grant no. (FP-109-43).

References

Adamian, A., Safari, K.H., Sheikholeslami, M., Habibi, M., Al-Furjan, M. and Chen, G. (2020), "Critical temperature and frequency characteristics of gpls-reinforced composite doubly curved panel", *Appl. Sci.*, **10**(9), 3251. https://doi.org/10.3390/app10093251.

Al-Furjan, M., Dehini, R., Khorami, M., Habibi, M. and won Jung, D. (2020a), "On the dynamics of the ultra-fast rotating cantilever orthotropic piezoelectric nanodisk based on nonlocal

strain gradient theory", *Compos. Struct.*, 112990. https://doi.org/10.1016/j.compstruct.2020.112990.

Al-Furjan, M., Fereidouni, M., Habibi, M., Abd Ali, R., Ni, J. and Safarpour, M. (2020b), "Influence of in-plane loading on the vibrations of the fully symmetric mechanical systems via dynamic simulation and generalized differential quadrature framework", *Eng. Comput.* 1-23. https://doi.org/10.1007/s00366-020-01177-7.

Al-Furjan, M., Fereidouni, M., Sedghiyan, D., Habibi, M. and won Jung, D. (2020c), "Three-dimensional frequency response of the CNT-Carbon-Fiber reinforced laminated circular/annular plates under initially stresses", *Compos. Struct.*, 113146. https://doi.org/10.1016/j.compstruct.2020.113146.

Al-Furjan, M., Habibi, M., Ghabussi, A., Safarpour, H., Safarpour, M. and Tounsi, A. (2020d), "Non-polynomial framework for stress and strain response of the FG-GPLRC disk using three-dimensional refined higher-order theory", *Eng. Struct.*, 111496. https://doi.org/10.1016/j.engstruct.2020.111496.

Al-Furjan, M., Habibi, M., won Jung, D. and Safarpour, H. (2020e), "Vibrational characteristics of a higher-order laminated composite viscoelastic annular microplate via modified couple stress theory", *Compos. Struct.*, 113152. https://doi.org/10.1016/j.compstruct.2020.113152.

Al-Furjan, M., Moghadam, S.A., Dehini, R., Shan, L., Habibi, M. and Safarpour, H. (2020f), "Vibration control of a smart shell reinforced by graphene nanoplatelets under external load: Semi-numerical and finite element modeling", *Thin Wall Struct.*, **159**, 107242. https://doi.org/10.1016/j.tws.2020.107242.

Al-Furjan, M., Oyarhossein, M.A., Habibi, M., Safarpour, H. and Jung, D.W. (2020g), "Frequency and critical angular velocity characteristics of rotary laminated cantilever microdisk via two-dimensional analysis", *Thin Wall Struct.*, **157**, 107111. https://doi.org/10.1016/j.tws.2020.107111.

Alipour, M., Torabi, M.A., Sareban, M., Lashini, H., Sadeghi, E., Fazaeli, A., Habibi, M. and Hashemi, R. (2020), "Finite element and experimental method for analyzing the effects of martensite morphologies on the formability of DP steels", *Mech. Based Des. Struct.*, **48**(5), 525-541. https://doi.org/10.1080/15397734.2019.1633343.

Arefi, M. (2018), "Analysis of a doubly curved piezoelectric nano shell: nonlocal electro-elastic bending solution", *Eur. J. Mech. A Solid.*, **70**, 226-237. https://doi.org/10.1016/j.euromechsol.2018.02.012.

Azoti, W. and Elmarakbi, A. (2019), "A multiscale approach for the nonlinear mechanical response of 3-phases fiber reinforced graphene nanoplatelets polymer composite materials", *Macromol. Theory Simul.*, **28**(4), 1900011. https://doi.org/10.1002/mats.201900011.

Bai, Y., Alzahrani, B., Baharom, S. and Habibi, M. (2020), "Semi-numerical simulation for vibrational responses of the viscoelastic imperfect annular system with honeycomb core under residual pressure", *Eng. Comput.*, 1-26. https://doi.org/10.1007/s00366-020-01191-9.

Barooti, M.M., Safarpour, H. and Ghadiri, M. (2017), "Critical speed and free vibration analysis of spinning 3D single-walled carbon nanotubes resting on elastic foundations", *Eur. Phys. J. Plus*, **132**(1), 6. https://doi.org/10.1140/epjp/i2017-11275-5.

Bellman, R. and Casti, J. (1971), "Differential quadrature and long-term integration", *J. Math. Anal. Appl.*, **34**(2), 235-238. https://doi.org/10.1016/j.tws.2020.107111.

Bellman, R., Kashef, B. and Casti, J. (1972), "Differential quadrature: A technique for the rapid solution of nonlinear partial differential equations", *J. Comput. Phys.*, **10**(1), 40-52. https://doi.org/10.1016/0021-9991(72)90089-7.

Checchetto, R., Miotello, A., Nicolais, L. and Carotenuto, G. (2014), "Gas transport through nanocomposite membrane composed by polyethylene with dispersed graphite nanoplatelets", *J. Membr. Sci.*, **463**, 196-204. https://doi.org/10.1016/j.memsci.2014.03.065.

Cheshmeh, E., Karbon, M., Eyvazian, A., Jung, D.w., Habibi, M. and Safarpour, M. (2020), "Buckling and vibration analysis of FG-CNTRC plate subjected to thermo-mechanical load based on higher order shear deformation theory", *Mech. Based Des. Struct.*, 1-24. https://doi.org/10.1080/15397734.2020.1744005.

Dai, H. and Safarpour, H. (2021a), "Frequency and thermal buckling information of laminated composite doubly curved open nanoshell", *Adv. Nano Res.*, **10**(1), 1-14. https://doi.org/10.12989/anr.2021.10.1.001.

Dai, Z., Zhang, L., Bolandi, S.Y. and Habibi, M. (2021b), "On the vibrations of the non-polynomial viscoelastic composite open-type shell under residual stresses", *Compos. Struct.*, 113599. https://doi.org/10.1016/j.compstruct.2021.113599.

Dehkordi, S.F. and Beni, Y.T. (2017), "Electro-mechanical free vibration of single-walled piezoelectric/flexoelectric nano cones using consistent couple stress theory", *Int. J. Mech. Sci.*, **128**, 125-139. https://doi.org/10.1016/j.ijmecsci.2017.04.004.

Dehshahri, K., Nejad, M.Z., Ziaee, S., Niknejad, A. and Hadi, A. (2020), "Free vibrations analysis of arbitrary three-dimensionally FGM nanoplates", *Adv. Nano Res.*, **8**(2), 115-134. https://doi.org/10.12989/anr.2020.8.2.115.

Ebrahimi, F., Habibi, M. and Safarpour, H. (2019a), "On modeling of wave propagation in a thermally affected GNP-reinforced imperfect nanocomposite shell", *Eng. Comput.*, **35**(4), 1375-1389. https://doi.org/10.1007/s00366-018-0669-4.

Ebrahimi, F., Hajilak, Z.E., Habibi, M. and Safarpour, H. (2019b), "Buckling and vibration characteristics of a carbon nanotube-reinforced spinning cantilever cylindrical 3D shell conveying viscous fluid flow and carrying spring-mass systems under various temperature distributions", *Proceedings of the Institution of Mechanical Engineers, Part C: Journal of Mechanical Engineering Science*, **233**(13), 4590-4605. https://doi.org/10.1177/0954406219832323.

Ebrahimi, F., Hashemabadi, D., Habibi, M. and Safarpour, H. (2020a), "Thermal buckling and forced vibration characteristics of a porous GNP reinforced nanocomposite cylindrical shell", *Microsyst. Technol.*, **26**(2), 461-473. https://doi.org/10.1007/s00542-019-04542-9.

Ebrahimi, F. and Jafari, A. (2017), "Investigating vibration behavior of smart imperfect functionally graded beam subjected to magnetic-electric fields based on refined shear deformation theory", *Adv. Nano Res.*, **5**(4), 281-301. https://doi.org/10.12989/anr.2017.5.4.281.

Ebrahimi, F., Karimiasl, M., Civalek, Ö. and Vinyas, M. (2019c), "Surface effects on scale-dependent vibration behavior of flexoelectric sandwich nanobeams", *Adv. Nano Res.*, **7**(2), 77-88. https://doi.org/10.12989/anr.2019.7.2.077.

Ebrahimi, F., Karimiasl, M. and Mahesh, V. (2019d), "Vibration analysis of magneto-flexo-electrically actuated porous rotary nanobeams considering thermal effects via nonlocal strain gradient elasticity theory", *Adv. Nano Res.*, **7**(4), 223-231. https://doi.org/10.12989/anr.2019.7.4.223.

Ebrahimi, F., Mohammadi, K., Barouti, M.M. and Habibi, M. (2019e), "Wave propagation analysis of a spinning porous graphene nanoplatelet-reinforced nanoshell", *Wave. Random Complex.*, 1-27. https://doi.org/10.1080/17455030.2019.1694729.

Ebrahimi, F. and Safarpour, H. (2018), "Vibration analysis of inhomogeneous nonlocal beams via a modified couple stress theory incorporating surface effects", *Wind Struct.*, **27**(6), 431-438. https://doi.org/10.12989/was.2018.27.6.431.

Ebrahimi, F. and Salari, E. (2019f), "Effect of non-uniform temperature distributions on nonlocal vibration and buckling of inhomogeneous size-dependent beams", *Adv. Nano Res.*, **6**(4), 377. https://doi.org/10.12989/anr.2018.6.4.377.

Ebrahimi, F., Supeni, E.E.B., Habibi, M. and Safarpour, H. (2020b), "Frequency characteristics of a GPL-reinforced composite microdisk coupled with a piezoelectric layer", *Eur. Phys. J. Plus*, **135**(2), 144. https://doi.org/10.1140/epjp/s13360-020-00217-x.

Eftekhar, H., Zeynali, H. and Nasihatgozar, M. (2018), "Electro-magneto temperature-dependent vibration analysis of functionally graded-carbon nanotube-reinforced piezoelectric Mindlin cylindrical shells resting on a temperature-dependent, orthotropic elastic medium", *Mech. Adv. Mater. Struct.*, **25**(1), 1-14. https://doi.org/10.12989/anr.2019.7.2.077.

Ehyaei, J. and Daman, M. (2017), "Free vibration analysis of double walled carbon nanotubes embedded in an elastic medium with initial imperfection", *Adv. Nano Res.*, **5**(2), 179-192. https://doi.org/10.12989/anr.2017.5.2.179.

Emdadi, M., Mohammadimehr, M. and Navi, B.R. (2019), "Free vibration of an annular sandwich plate with CNTRC facesheets and FG porous cores using Ritz method", *Adv. Nano Res.*, **7**(2), 109-123. https://doi.org/10.12989/anr.2019.7.2.109.

Esmailpoor Hajilak, Z., Pourghader, J., Hashemabadi, D., Sharifi Bagh, F., Habibi, M. and Safarpour, H. (2019), "Multilayer GPLRC composite cylindrical nanoshell using modified strain gradient theory", *Mech. Based Des. Struct.*, **47**(5), 521-545. https://doi.org/10.1080/15397734.2019.1566743.

Fan, J., Huang, J., Ding, J. and Zhang, J. (2017), "Free vibration of functionally graded carbon nanotube-reinforced conical panels integrated with piezoelectric layers subjected to elastically restrained boundary conditions", *Adv. Mech. Eng.*, **9**(7), 1687814017711811. https://doi.org/10.1177/1687814017711811.

Fang, J. and Zhou, D. (2017), "Free vibration analysis of rotating mindlin plates with variable thickness", *Int. J. Struct. Stabil. Dynam.*, **17**(4), 1750046. https://doi.org/10.1142/S0219455417500468.

Feng, C., Kitipornchai, S. and Yang, J. (2017), "Nonlinear bending of polymer nanocomposite beams reinforced with non-uniformly distributed graphene platelets (GPLs)", *Compos. Part B Eng.*, **110**, 132-140. https://doi.org/10.1016/j.compositesb.2016.11.024.

Ghabussi, A., Ashrafi, N., Shavalipour, A., Hosseinpour, A., Habibi, M., Moayedi, H., Babaei, B. and Safarpour, H. (2019), "Free vibration analysis of an electro-elastic GPLRC cylindrical shell surrounded by viscoelastic foundation using modified length-couple stress parameter", *Mech. Based Des. Struct.*, 1-25. https://doi.org/10.1080/15397734.2019.1705166.

Ghabussi, A., Habibi, M., NoormohammadiArani, O., Shavalipour, A., Moayedi, H. and Safarpour, H. (2020), "Frequency characteristics of a viscoelastic graphene nanoplatelet–reinforced composite circular microplate", *J. Vib. Control.*, 1077546320923930. https://doi.org/10.1177/1077546320923930.

Ghadiri, M. and Safarpour, H. (2016a), "Free vibration analysis of embedded magneto-electro-thermo-elastic cylindrical nanoshell based on the modified couple stress theory", *Appl. Phys. A.*, **122**(9), 1-11. https://doi.org/10.1007/s00339-016-0365-4.

Ghadiri, M. and Safarpour, H. (2016b), "Free vibration analysis of embedded magneto-electro-thermo-elastic cylindrical nanoshell based on the modified couple stress theory", *Appl. Phys. A.*, **122**(9), 833. https://doi.org/10.1007/s00339-016-0365-4.

Ghannadpour, S. and Moradi, F. (2019), "Nonlocal nonlinear analysis of nano-graphene sheets under compression using semi-Galerkin technique", *Adv. Nano Res.*, **7**(5), 311-324. https://doi.org/10.12989/anr.2019.7.5.311.

Ghazanfari, A., Soleimani, S.S., Keshavarzzadeh, M., Habibi, M., Assempuor, A. and Hashemi, R. (2020), "Prediction of FLD for sheet metal by considering through-thickness shear stresses", *Mech. Based Des. Struct.*, **48**(6), 755-772. https://doi.org/10.1080/15397734.2019.1662310.

Guo, Y., Mi, H. and Habibi, M. (2021), "Electromechanical energy absorption, resonance frequency, and low-velocity impact analysis of the piezoelectric doubly curved system", *Mech. Syst. Signal Proc.*, **157**, 107723. https://doi.org/10.1016/j.ymssp.2021.107723.

Habibi, M., Ghazanfari, A., Assempour, A., Naghdabadi, R. and Hashemi, R. (2017), "Determination of forming limit diagram using two modified finite element models", *Mech. Eng.*, **48**(4), 141-144. https://doi.org/10.22060/MEJ.2016.664.

Habibi, M., Hashemabadi, D. and Safarpour, H. (2019), "Vibration analysis of a high-speed rotating GPLRC nanostructure coupled with a piezoelectric actuator", *Eur. Phys. J. Plus*, **134**(6), 307. https://doi.org/10.1140/epjp/i2019-12742-7.

Habibi, M., Hashemi, R., Ghazanfari, A., Naghdabadi, R. and Assempour, A. (2018a), "Forming limit diagrams by including the M–K model in finite element simulation considering the effect of bending", *Proceedings of the Institution of Mechanical Engineers, Part L: Journal of Materials: Design and Applications*, **232**(8), 625-636. https://doi.org/10.1177/1464420716642258.

Habibi, M., Hashemi, R., Sadeghi, E., Fazaeli, A., Ghazanfari, A. and Lashini, H. (2016), "Enhancing the mechanical properties and formability of low carbon steel with dual-phase microstructures", *J. Mater. Eng. Perform.*, **25**(2), 382-389. https://doi.org/10.1007/s11665-016-1882-1.

Habibi, M., Hashemi, R., Tafti, M.F. and Assempour, A. (2018b), "Experimental investigation of mechanical properties, formability and forming limit diagrams for tailor-welded blanks produced by friction stir welding", *J. Manufact. Proc.*, **31**, 310-323. https://doi.org/10.1016/j.jmapro.2017.11.009.

Habibi, M., Mohammadgholiha, M. and Safarpour, H. (2019a), "Wave propagation characteristics of the electrically GNP-reinforced nanocomposite cylindrical shell", *J. Brazil. Soc. Mech. Sci. Eng.*, **41**(5), 221. https://doi.org/10.1007/s40430-019-1715-x.

Habibi, M., Mohammadi, A., Safarpour, H. and Ghadiri, M. (2019b), "Effect of porosity on buckling and vibrational characteristics of the imperfect GPLRC composite nanoshell", *Mech. Based Des. Struct.*, 1-30. https://doi.org/10.1080/15397734.2019.1701490.

Habibi, M., Mohammadi, A., Safarpour, H., Shavalipour, A. and Ghadiri, M. (2019c), "Wave propagation analysis of the laminated cylindrical nanoshell coupled with a piezoelectric actuator", *Mech. Based Des. Struct.*, 1-19. https://doi.org/10.1080/15397734.2019.1697932.

Habibi, M., Safarpour, M. and Safarpour, H. (2020), "Vibrational characteristics of a FG-GPLRC viscoelastic thick annular plate using fourth-order Runge-Kutta and GDQ methods", *Mech. Based Des. Struct.*, 1-22. https://doi.org/10.1080/15397734.2020.1779086.

Habibi, M., Taghdir, A. and Safarpour, H. (2019d), "Stability analysis of an electrically cylindrical nanoshell reinforced with graphene nanoplatelets", *Compos. Part B Eng.*, **175**, 107125. https://doi.org/10.1016/j.compositesb.2019.107125.

Hashemi, H.R., Alizadeh, A.A., Oyarhossein, M.A., Shavalipour, A., Makkiabadi, M. and Habibi, M. (2019), "Influence of imperfection on amplitude and resonance frequency of a reinforcement compositionally graded nanostructure", *Wave. Random Complex.*, 1-27. https://doi.org/10.1080/17455030.2019.1662968.

Hou, F., Wu, S., Moradi, Z. and Shafiei, N. (2021), "The computational modeling for the static analysis of axially functionally graded micro-cylindrical imperfect beam applying the computer simulation", *Eng. Comput.*, 1-19. https://doi.org/10.1080/17455030.2019.1662968.

Huang, X., Zhang, Y., Moradi, Z. and Shafiei, N. (2021a), "Computer simulation via a couple of homotopy perturbation

methods and the generalized differential quadrature method for nonlinear vibration of functionally graded non-uniform micro-tube", *Eng. Comput.*, 1-18. https://doi.org/10.1007/s00366-021-01395-7.

Huang, X., Zhu, Y., Vafaei, P., Moradi, Z. and Davoudi, M. (2021b), "An iterative simulation algorithm for large oscillation of the applicable 2D-electrical system on a complex nonlinear substrate", *Eng. Comput.*, 1-13. https://doi.org/10.1007/s00366-021-01320-y.

Jermsittiparsert, K., Ghabussi, A., Forooghi, A., Shavalipour, A., Habibi, M., won Jung, D. and Safa, M. (2020), "Critical voltage, thermal buckling and frequency characteristics of a thermally affected GPL reinforced composite microdisk covered with piezoelectric actuator", *Mech. Based Des. Struct.*, 1-23. https://doi.org/10.1080/15397734.2020.1748052.

Jiao, J., Ghoreishi, S.-m., Moradi, Z. and Oslub, K. (2021), "Coupled particle swarm optimization method with genetic algorithm for the static–dynamic performance of the magneto-electro-elastic nanosystem", *Eng. Comput.*, 1-23. https://doi.org/10.1007/s00366-021-01391-x.

Ke, L.L., Wang, Y.S., Yang, J. and Kitipornchai, S. (2014a), "The size-dependent vibration of embedded magneto-electro-elastic cylindrical nanoshells", *Smart Mater. Struct.*, **23**(12), 125036. https://doi.org/10.1080/17455030.2019.1662968.

Ke, L., Wang, Y. and Reddy, J. (2014b), "Thermo-electro-mechanical vibration of size-dependent piezoelectric cylindrical nanoshells under various boundary conditions", *Compos. Struct.*, **116**, 626-636. https://doi.org/10.1016/j.compstruct.2014.05.048.

Khalili, S. and Mohammadi, Y. (2012), "Free vibration analysis of sandwich plates with functionally graded face sheets and temperature-dependent material properties: A new approach", *Eur. J. Mech. A Solid.*, **35**, 61-74. https://doi.org/10.1007/s00366-021-01395-7.

Kheibari, F. and Beni, Y.T. (2017), "Size dependent electro-mechanical vibration of single-walled piezoelectric nanotubes using thin shell model", *Mater. Des.*, **114**, 572-583. https://doi.org/10.1016/j.apm.2018.04.015.

Kumar, B.R. (2018), "Investigation on mechanical vibration of double-walled carbon nanotubes with inter-tube Van der waals forces", *Adv. Nano Res.*, **6**(2), 135. https://doi.org/10.12989/anr.2018.6.2.135.

Li, Y., Li, S., Guo, K., Fang, X. and Habibi, M. (2020), "On the modeling of bending responses of graphene-reinforced higher order annular plate via two-dimensional continuum mechanics approach", *Eng. Comput.*, 1-22. https://doi.org/10.1080/15397734.2020.1779086.

Liu, D., Kitipornchai, S., Chen, W. and Yang, J. (2018), "Three-dimensional buckling and free vibration analyses of initially stressed functionally graded graphene reinforced composite cylindrical shell", *Compos. Struct.*, **189**, 560-569. https://doi.org/10.1016/j.compstruct.2018.01.106.

Liu, H., Shen, S., Oslub, K., Habibi, M. and Safarpour, H. (2021a), "Amplitude motion and frequency simulation of a composite viscoelastic microsystem within modified couple stress elasticity", *Eng. Comput.*, 1-15. https://doi.org/10.1007/s00366-021-01316-8.

Liu, Y., Wang, W., He, T., Moradi, Z. and Larco Benítez, M.A. (2021b), "On the modelling of the vibration behaviors via discrete singular convolution method for a high-order sector annular system", *Eng. Comput.*, 1-23. https://doi.org/10.1080/15397734.2020.1779086.

Lori, E.S., Ebrahimi, F., Supeni, E.E.B., Habibi, M. and Safarpour, H. (2020), "The critical voltage of a GPL-reinforced composite microdisk covered with piezoelectric layer", *Eng. Comput.*, 1-20. https://doi.org/10.1007/s00366-020-01004-z.

Ma, L., Liu, X. and Moradi, Z. (2021), "On the chaotic behavior of graphene-reinforced annular systems under harmonic excitation", *Eng. Comput.*, 1-25. https://doi.org/10.1007/s00366-020-01210-9.

Mahinzare, M., Ranjbarpur, H. and Ghadiri, M. (2018), "Free vibration analysis of a rotary smart two directional functionally graded piezoelectric material in axial symmetry circular nanoplate", *Mech. Syst. Signal Proc.*, **100**, 188-207. https://doi.org/10.1016/j.ymssp.2017.07.041.

Moayedi, H., Aliakbarlou, H., Jebeli, M., Noormohammadiarani, O., Habibi, M., Safarpour, H. and Foong, L. (2020a), "Thermal buckling responses of a graphene reinforced composite micropanel structure", *Int. J. Appl. Mech.*, **12**(1), 2050010. https://doi.org/10.1142/S1758825120500106.

Moayedi, H., Darabi, R., Ghabussi, A., Habibi, M. and Foong, L.K. (2020b), "Weld orientation effects on the formability of tailor welded thin steel sheets", *Thin Wall Struct.*, **149**, 106669. https://doi.org/10.1016/j.tws.2020.106669.

Moayedi, H., Ebrahimi, F., Habibi, M., Safarpour, H. and Foong, L.K. (2020c), "Application of nonlocal strain–stress gradient theory and GDQEM for thermo-vibration responses of a laminated composite nanoshell", *Eng. Comput.*, 1-16. https://doi.org/10.1007/s00366-020-01002-1.

Moayedi, H., Habibi, M., Safarpour, H., Safarpour, M. and Foong, L. (2019), "Buckling and frequency responses of a graphene nanoplatelet reinforced composite microdisk", *Int. J. Appl. Mech.*, **11**(10), 1950102. https://doi.org/10.1142/S1758825119501023.

Mohammadgholiha, M., Shokrgozar, A., Habibi, M. and Safarpour, H. (2019), "Buckling and frequency analysis of the nonlocal strain–stress gradient shell reinforced with graphene nanoplatelets", *J. Vib. Control.*, **25**(19-20), 2627-2640. https://doi.org/10.1177/1077546319863251.

Mohammadi, A., Lashini, H., Habibi, M. and Safarpour, H. (2019a), "Influence of viscoelastic foundation on dynamic behaviour of the double walled cylindrical inhomogeneous micro shell using MCST and with the aid of GDQM", *J. Solid Mech.*, **11**(2), 440-453. https://doi.org/10.22034/jsm.2019.665264.

Mohammadimehr, M., Okhravi, S. and Akhavan Alavi, S. (2018), "Free vibration analysis of magneto-electro-elastic cylindrical composite panel reinforced by various distributions of CNTs with considering open and closed circuits boundary conditions based on FSDT", *J. Vib. Control.*, **24**(8), 1551-1569. https://doi.org/10.1016/j.ymssp.2017.07.041.

Moradi, Z., Davoudi, M., Ebrahimi, F. and Ehyaei, A.F. (2021), "Intelligent wave dispersion control of an inhomogeneous micro-shell using a proportional-derivative smart controller", *Wave. Random Complex.*, 1-24. https://doi.org/10.1016/j.tws.2020.106669.

Najaafi, N., Jamali, M., Habibi, M., Sadeghi, S., Jung, D.w. and Nabipour, N. (2020), "Dynamic instability responses of the substructure living biological cells in the cytoplasm environment using stress-strain size-dependent theory", *J. Biomol. Struct. Dynam.*, 1-12. https://doi.org/10.1080/07391102.2020.1751297.

Nasihatgozar, M. and Khalili, S. (2017), "Free vibration of a thick sandwich plate using higher order shear deformation theory and DQM for different boundary conditions", *J. Appl. Comput. Mech.*, **3**(1), 16-24. https://doi.org/10.22055/JACM.2017.12548.

Ninh, D.G. and Bich, D.H. (2018), "Characteristics of nonlinear vibration of nanocomposite cylindrical shells with piezoelectric actuators under thermo-mechanical loads", *Aerosp. Sci. Technol.*, **77**, 595-609. https://doi.org/10.1016/j.ast.2018.04.008.

Oyarhossein, M.A., Alizadeh, A.a., Habibi, M., Makkiabadi, M., Daman, M., Safarpour, H. and Jung, D.W. (2020), "Dynamic response of the nonlocal strain-stress gradient in laminated polymer composites microtubes", *Sci. Rep.*, **10**(1), 1-19.

https://doi.org/10.1038/s41598-020-61855-w.

Pourjabari, A., Hajilak, Z.E., Mohammadi, A., Habibi, M. and Safarpour, H. (2019), "Effect of porosity on free and forced vibration characteristics of the GPL reinforcement composite nanostructures", *Comput. Math. Appl.*, 77(10), 2608-2626. https://doi.org/10.1016/j.camwa.2018.12.041.

Pourmoayed, A., Fard, K.M. and Shahravi, M. (2017), "Vibration analysis of a cylindrical sandwich panel with flexible core using an improved higher-order theory", *Latin Am. J. Solid Struct.*, **14**(4), 714-742. http://dx.doi.org/10.1590/1679-78253410.

Rafiee, M.A., Rafiee, J., Wang, Z., Song, H., Yu, Z.Z. and Koratkar, N. (2009), "Enhanced mechanical properties of nano-composites at low graphene content", *ACS Nano*, **3**(12), 3884-3890. https://doi.org/10.1021/nn9010472.

Rajasekaran, S. (2009), *Structural Dynamics of Earthquake Engineering: Theory and Application Using MATHEMATICA and MATLAB*, Elsevier.

Razavi, H., Babadi, A.F. and Beni, Y.T. (2017), "Free vibration analysis of functionally graded piezoelectric cylindrical nano-shell based on consistent couple stress theory", *Compos. Struct.*, **160**, 1299-1309. https://doi.org/10.1016/j.compstruct.2016.10.056.

SafarPour, H. and Ghadiri, M. (2017a), "Critical rotational speed, critical velocity of fluid flow and free vibration analysis of a spinning SWCNT conveying viscous fluid", *Microfluid. Nanofluid.*, **21**(2), 22. https://doi.org/10.1007/s10404-017-1858-y.

Safarpour, H., Ghanizadeh, S.A. and Habibi, M. (2018), "Wave propagation characteristics of a cylindrical laminated composite nanoshell in thermal environment based on the nonlocal strain gradient theory", *Eur. Phys. J. Plus*, **133**(12), 532. https://doi.org/10.1140/epjp/i2018-12385-2.

Safarpour, H., Hajilak, Z.E. and Habibi, M. (2019a), "A size-dependent exact theory for thermal buckling, free and forced vibration analysis of temperature dependent FG multilayer GPLRC composite nanostructures restring on elastic foundation", *Int. J. Mech. Mater. Des.*, 15(3), 569-583. https://doi.org/10.1007/s10999-018-9431-8.

SafarPour, H., Hosseini, M. and Ghadiri, M. (2017b), "Influence of three-parameter viscoelastic medium on vibration behavior of a cylindrical nonhomogeneous microshell in thermal environment: An exact solution", *J. Therm. Stress.*, **40**(11), 1353-1367. https://doi.org/10.1080/01495739.2017.1350827.

SafarPour, H., Mohammadi, K., Ghadiri, M. and Rajabpour, A. (2017c), "Influence of various temperature distributions on critical speed and vibrational characteristics of rotating cylindrical microshells with modified lengthscale parameter", *Eur. Phys. J. Plus*, **132**(6), 1-19. https://doi.org/10.1140/epjp/i2017-11551-4.

Safarpour, H., Pourghader, J. and Habibi, M. (2019b), "Influence of spring-mass systems on frequency behavior and critical voltage of a high-speed rotating cantilever cylindrical three-dimensional shell coupled with piezoelectric actuator", *J. Vib. Control.*, **25**(9), 1543-1557. https://doi.org/10.1177/1077546319828465.

Safarpour, M., Ebrahimi, F., Habibi, M. and Safarpour, H. (2020a), "On the nonlinear dynamics of a multi-scale hybrid nanocomposite disk", *Eng. Comput.*, 1-20. https://doi.org/10.1007/s00366-020-00949-5.

Safarpour, M., Ghabussi, A., Ebrahimi, F., Habibi, M. and Safarpour, H. (2020b), "Frequency characteristics of FG-GPLRC viscoelastic thick annular plate with the aid of GDQM", *Thin Wall Struct.*, **150**, 106683. https://doi.org/10.1016/j.tws.2020.106683.

Salari, F.E.E. (2016), "Thermal loading effects on electro-mechanical vibration behavior of piezoelectrically actuated inhomogeneous size-dependent Timoshenko nanobeams", *Adv. Nano Res.*, **4**(3), 197-228. https://doi.org/10.12989/anr.2016.4.3.197.

Shahsavari, D., Karami, B. and Janghorban, M. (2019), "Size-dependent vibration analysis of laminated composite plates", *Adv. Nano Res.*, 7(5), 337-349. https://doi.org/10.12989/anr.2019.7.5.337.

Shariati, M., Sulong, N.R. and Khanouki, M.A. (2012), "Experimental assessment of channel shear connectors under monotonic and fully reversed cyclic loading in high strength concrete", *Mater Des.*, **34**, 325-331. https://doi.org/10.1016/j.matdes.2011.08.008.

Shariati, M., Sulong, N.R., Shariati, A. and Khanouki, M.A. (2016a), "Behavior of V-shaped angle shear connectors: experimental and parametric study", *Mater. Struct.*, **49**(9), 3909-3926. https://doi.org/10.1617/s11527-015-0762-8.

Shariati, M., Sulong, N.R., Shariati, A. and Kueh, A. (2016b), "Comparative performance of channel and angle shear connectors in high strength concrete composites: An experimental study", *Constr. Build. Mater.*, **120**, 382-392. https://doi.org/10.1016/j.conbuildmat.2016.05.102.

Shariati, M., Faegh, S.S., Mehrabi, P., Bahavarnia, S., Zandi, Y., Masoom, D.R., Toghroli, A., Trung, N.T. and Salih, M.N. (2019), "Numerical study on the structural performance of corrugated low yield point steel plate shear walls with circular openings", *Steel Compos. Struct.*, **33**(4), 569-581. https://doi.org/10.12989/scs.2019.33.4.569.

Shariati, A., Ghabussi, A., Habibi, M., Safarpour, H., Safarpour, M., Tounsi, A. and Safa, M. (2020a), "Extremely large oscillation and nonlinear frequency of a multi-scale hybrid disk resting on nonlinear elastic foundation", *Thin Wall Struct.*, **154**, 106840. https://doi.org/10.1016/j.tws.2020.106840.

Shariati, A., Habibi, M., Tounsi, A., Safarpour, H. and Safa, M. (2020b), "Application of exact continuum size-dependent theory for stability and frequency analysis of a curved cantilevered microtubule by considering viscoelastic properties", *Eng. Comput.*, 1-20. https://doi.org/10.1007/s00366-020-01024-9.

Shariati, A., Mohammad-Sedighi, H., Żur, K.K., Habibi, M. and Safa, M. (2020c), "On the vibrations and stability of moving viscoelastic axially functionally graded nanobeams", *Materials*, **13**(7), 1707. https://doi.org/10.3390/ma13071707.

Shariati, A., Mohammad-Sedighi, H., Żur, K.K., Habibi, M. and Safa, M. (2020d), "Stability and dynamics of viscoelastic moving rayleigh beams with an asymmetrical distribution of material parameters", *Symmetry*, **12**(4), 586. https://doi.org/10.3390/sym12040586.

Shariati, M., Azar, S.M., Arjomand, M.A., Tehrani, H.S., Daei, M. and Safa, M. (2020e), "Evaluating the impacts of using piles and geosynthetics in reducing the settlement of fine-grained soils under static load", *Geomech. Eng.*, **20**(2), 87-101. https://doi.org/10.12989/gae.2020.20.2.087.

Shariati, M., Ghorbani, M., Naghipour, M., Alinejad, N. and Toghroli, A. (2020f), "The effect of RBS connection on energy absorption in tall buildings with braced tube frame system", *Steel Compos. Struct.*, **34**(3), 393-407. https://doi.org/10.12989/scs.2020.34.3.393.

Shariati, M., Lagzian, M., Maleki, S., Shariati, A. and Trung, N.T. (2020g), "Evaluation of seismic performance factors for tension-only braced frames", *Steel Compos. Struct.*, **35**(4), 599-609. https://doi.org/10.12989/scs.2020.35.4.599.

Shariati, M., Mafipour, M.S., Ghahremani, B., Azarhomayun, F., Ahmadi, M., Trung, N.T. and Shariati, A. (2020h), "A novel hybrid extreme learning machine–grey wolf optimizer (ELM-GWO) model to predict compressive strength of concrete with partial replacements for cement", *Eng. Comput.*, 1-23. https://doi.org/10.1007/s00366-020-01081-0.

Shariati, M., Mafipour, M.S., Mehrabi, P., Ahmadi, M., Wakil, K.,

Trung, N.T. and Toghroli, A. (2020i), "Prediction of concrete strength in presence of furnace slag and fly ash using Hybrid ANN-GA (Artificial Neural Network-Genetic Algorithm)", *Smart Struct. Syst.*, **25**(2), 183-195. https://doi.org/10.12989/sss.2020.25.2.183.

Shariati, M., Naghipour, M., Yousofizinsaz, G., Toghroli, A. and Tabarestani, N.P. (2020j), "Numerical study on the axial compressive behavior of built-up CFT columns considering different welding lines", *Steel Compos. Struct.*, **34**(3), 377-391. http://doi.org/10.12989/scs.2020.34.3.377.

Shariati, M., Tahmasbi, F., Mehrabi, P., Bahadori, A. and Toghroli, A. (2020k), "Monotonic behavior of C and L shaped angle shear connectors within steel-concrete composite beams: An experimental investigation", *Steel Compos Struct.*, **35**(2), 237-247. http://doi.org/10.12989/scs.2020.35.2.237.

Shariati, M., Davoodnabi, S.M., Toghroli, A., Kong, Z. and Shariati, A. (2021a), "Hybridization of metaheuristic algorithms with adaptive neuro-fuzzy inference system to predict load-slip behavior of angle shear connectors at elevated temperatures", *Compos. Struct.*, 114524. https://doi.org/10.1016/j.compstruct.2021.114524.

Shariati, M., Shariati, A., Trung, N.T., Shoaei, P., Ameri, F., Bahrami, N. and Zamanabadi, S.N. (2021b), "Alkali-activated slag (AAS) paste: Correlation between durability and microstructural characteristics", *Constr. Build. Mater.*, **267**, 120886. https://doi.org/10.1016/j.conbuildmat.2020.120886.

Shi, G., Araby, S., Gibson, C.T., Meng, Q., Zhu, S. and Ma, J. (2018), "Graphene platelets and their polymer composites: Fabrication, structure, properties, and applications", *Adv. Funct. Mater.*, **28**(19), 1706705. https://doi.org/10.1016/j.apm.2018.04.015.

Shi, X., Li, J. and Habibi, M. (2020), "On the statics and dynamics of an electro-thermo-mechanically porous GPLRC nanoshell conveying fluid flow", *Mech. Based Des. Struct.*, 1-37. https://doi.org/10.1080/15397734.2020.1772088.

Shojaeefard, M., Mahinzare, M., Safarpour, H., Googarchin, H.S. and Ghadiri, M. (2018), "Free vibration of an ultra-fast-rotating-induced cylindrical nano-shell resting on a Winkler foundation under thermo-electro-magneto-elastic condition", *Appl. Math. Modell.*, **61**, 255-279. https://doi.org/10.1016/j.apm.2018.04.015.

Shokrgozar, A., Ghabussi, A., Ebrahimi, F., Habibi, M. and Safarpour, H. (2020a), "Viscoelastic dynamics and static responses of a graphene nanoplatelets-reinforced composite cylindrical microshell", *Mech. Based Des. Struct.*, 1-28. https://doi.org/10.1080/15397734.2020.1719509.

Shokrgozar, A., Safarpour, H. and Habibi, M. (2020b), "Influence of system parameters on buckling and frequency analysis of a spinning cantilever cylindrical 3D shell coupled with piezoelectric actuator", *Proceedings of the Institution of Mechanical Engineers, Part C: Journal of Mechanical Engineering Science*, **234**(2), 512-529. https://doi.org/10.1177/0954406219883312.

Shu, C. (2012), *Differential Quadrature and Its Application in Engineering*, Springer Science & Business Media.

Shu, C. and Richards, B.E. (1992), "Application of generalized differential quadrature to solve two-dimensional incompressible Navier-Stokes equations", *Int. J. Numer. Method Fluid*, **15**(7), 791-798. https://doi.org/10.1002/fld.1650150704.

Singh, V.K. and Panda, S.K. (2017), "Geometrical nonlinear free vibration analysis of laminated composite doubly curved shell panels embedded with piezoelectric layers", *J. Vib. Control.*, **23**(13), 2078-2093. https://doi.org/10.1177/1099636215577363.

Song, M., Kitipornchai, S. and Yang, J. (2017), "Free and forced vibrations of functionally graded polymer composite plates reinforced with graphene nanoplatelets", *Compos. Struct.*, **159**, 579-588. https://doi.org/10.1016/j.compstruct.2016.09.070.

Sun, J. and Zhao, J. (2018), "Multi-layer graphene reinforced nano-laminated WC-Co composites", *Mater. Sci. Eng. A*, **723**, 1-7. https://doi.org/10.1039/D0GC02125C.

Tounsi, A., Benguediab, S., Semmah, A. and Zidour, M. (2013), "Nonlocal effects on thermal buckling properties of double-walled carbon nanotubes", *Adv. Nano Res.*, **1**(1), 1-11. https://doi.org/10.12989/anr.2013.1.1.001.

Wang, H., Zhang, H., Dousti, R. and Safarpour, H. (2021), "Dynamic simulation of moderately thick annular system coupled with shape memory alloy and multi-phase nano-composite face sheets", *Eng. Comput.* 1-24. https://doi.org/10.1007/s00366-020-01246-x.

Wang, Q. (2002), "On buckling of column structures with a pair of piezoelectric layers", *Eng. Struct.*, **24**(2), 199-205. https://doi.org/10.1016/S0141-0296(01)00088-8.

White, H. (1992), *Artificial Neural Networks: Approximation and Learning Theory*, Blackwell Publishers, New Jersey, U.S.A.

Wu, H., Kitipornchai, S. and Yang, J. (2017), "Thermal buckling and postbuckling of functionally graded graphene nano-composite plates", *Mater. Des.*, **132**, 430-441. https://doi.org/10.1016/j.matdes.2017.07.025.

Wu, C.P., Chen, Y.H., Hong, Z.L. and Lin, C.H. (2018), "Nonlinear vibration analysis of an embedded multi-walled carbon nanotube", *Adv. Nano Res.*, **6**(2), 163-182. https://doi.org/10.12989/anr.2018.6.2.163.

Xu, W., Pan, G., Moradi, Z. and Shafiei, N. (2021), "Nonlinear forced vibration analysis of functionally graded non-uniform cylindrical microbeams applying the semi-analytical solution", *Compos. Struct.*, 114395. https://doi.org/10.1016/j.compstruct.2021.114395.

Yang, J., Wu, H. and Kitipornchai, S. (2017), "Buckling and postbuckling of functionally graded multilayer graphene platelet-reinforced composite beams", *Compos. Struct.*, **161**, 111-118. https://doi.org/10.1016/j.compstruct.2016.11.048.

Yu, X., Maalla, A. and Moradi, Z. (2022), "Electroelastic high-order computational continuum strategy for critical voltage and frequency of piezoelectric NEMS via modified multi-physical couple stress theory", *Mech. Syst. Signal Proc.*, **165**, 108373. https://doi.org/10.1016/j.ymssp.2021.108373.

Zare, R., Najaafi, N., Habibi, M., Ebrahimi, F. and Safarpour, H. (2020), "Influence of imperfection on the smart control frequency characteristics of a cylindrical sensor-actuator GPLRC cylindrical shell using a proportional-derivative smart controller", *Smart Struct. Syst.*, **26**(4), 469-480. https://doi.org/10.12989/sss.2020.26.4.469.

Zeiler, M.D. (2012), "Adadelta: An adaptive learning rate method", arXiv preprint arXiv:1212.5701. https://doi.org/arXiv preprint arXiv:1212.5701.

Zhang, L., Chen, Z., Habibi, M., Ghabussi, A. and Alyousef, R. (2021a), "Low-velocity impact, resonance, and frequency responses of FG-GPLRC viscoelastic doubly curved panel", *Compos. Struct.*, **269**, 114000. https://doi.org/10.1016/j.compstruct.2021.114000.

Zhang, W., Liu, Z., Liang, Z., Oslub, K. and Safarpour, H. (2021b), "A comprehensive computer simulation of the size-dependent sector or complete microsystem via two-dimensional generalized differential quadrature method", *Eng. Comput.*, 1-17. https://doi.org/10.1007/s00366-021-01440-5.

Zhang, X., Shamsodin, M., Wang, H., NoormohammadiArani, O., Khan, A.M., Habibi, M. and Al-Furjan, M. (2021c), "Dynamic information of the time-dependent tobullian biomolecular structure using a high-accuracy size-dependent theory", *J. Biomol. Struct. Dynam.*, **39**(9), 3128-3143. https://doi.org/10.1080/07391102.2020.1760939.

Zhao, H., Wang, L., Issakhov, A. and Safarpour, H. (2021a), "Poroelasticity framework for stress/strain responses of the multi-phase circular/annular systems resting on various types of

elastic foundations", *Eur*. *Phys*. *J*. *Plus*, **136**(8), 1-44. https://doi.org/10.1140/epjp/s13360-021-01761-w.

Zhao, Y., Moradi, Z., Davoudi, M. and Zhuang, J. (2021b), "Bending and stress responses of the hybrid axisymmetric system via state-space method and 3D-elasticity theory", *Eng*. *Comput*., 1-23. https://doi.org/10.1007/s00366-020-01242-1.

Zhong, P.F., Lin, H.M., Wang, L.W., Mo, Z.Y., Meng, X.J., Tang, H.T. and Pan, Y.M. (2020), "Electrochemically enabled synthesis of sulfide imidazopyridines via a radical cyclization cascade", *Green Chem*., **22**(19), 6334-6339. https://doi.org/10.1039/D0GC02125C.

Zhu, C.S., Fang, X.Q., Liu, J.X. and Li, H.Y. (2017), "Surface energy effect on nonlinear free vibration behavior of orthotropic piezoelectric cylindrical nano-shells", *Eur*. *J*. *Mech*. *A Solid*., **66**, 423-432. https://doi.org/10.1016/j.compstruct.2021.114000.

Zhu, X., Lu, Z., Wang, Z., Xue, L. and Ebrahimi-Mamaghani, A. (2020), "Vibration of spinning functionally graded nanotubes conveying fluid", *Eng*. *Comput.*, 1-22. https://doi.org/10.1007/s00366-020-01123-7.

CC